

The subcommissural organ regulates brain development via secreted peptides

Received: 26 September 2022

Accepted: 3 April 2024

Published online: 13 May 2024

 Check for updates


Tingting Zhang^{1,2}, Daosheng Ai^{1,2}, Pingli Wei³, Ying Xu^{4,5}, Zhanying Bi^{2,6}, Fengfei Ma³, Fengzhi Li^{2,7}, Xing-jun Chen^{1,2}, Zhaohuan Zhang⁸, Xiaoxiao Zou^{2,9}, Zongpei Guo², Yue Zhao², Jun-Liszt Li^{1,2}, Meng Ye^{2,9,10}, Ziyang Feng², Xinshuang Zhang², Lijun Zheng^{2,10}, Jie Yu^{2,11}, Chunli Li¹², Tianqi Tu¹³, Hongkui Zeng¹⁴, Jianfeng Lei¹⁵, Hongqi Zhang¹³, Tao Hong¹³, Li Zhang², Benyan Luo¹¹, Zhen Li², Chao Xing¹⁶, Chenxi Jia⁵, Lingjun Li³  , Wenzhi Sun^{2,10}   & Woo-ping Ge^{2,9,13}  

The subcommissural organ (SCO) is a gland located at the entrance of the aqueduct of Sylvius in the brain. It exists in species as distantly related as amphioxus and humans, but its function is largely unknown. Here, to explore its function, we compared transcriptomes of SCO and non-SCO brain regions and found three genes, *Sspo*, *Car3* and *Spdef*, that are highly expressed in the SCO. Mouse strains expressing Cre recombinase from endogenous promoter/enhancer elements of these genes were used to genetically ablate SCO cells during embryonic development, resulting in severe hydrocephalus and defects in neuronal migration and development of neuronal axons and dendrites. Unbiased peptidomic analysis revealed enrichment of three SCO-derived peptides, namely, thymosin beta 4, thymosin beta 10 and NP24, and their reintroduction into SCO-ablated brain ventricles substantially rescued developmental defects. Together, these data identify a critical role for the SCO in brain development.

The subcommissural organ (SCO) is an evolutionarily conserved ependymal gland located under the posterior commissure of the brain at the entrance to the cerebral aqueduct above the third ventricle^{1–3}. So far, no specific transgenic mouse lines are available for gene manipulation in SCO cells. As such, most of our knowledge about SCO function has been gleaned from analyses of SCO lesions, animal models or observations of patients with naturally occurring defects in the brain regions containing the SCO^{4,5}. For example, H-Tx model rats develop congenital hydrocephalus⁶. Early studies indicated that such phenotypes are associated with abnormal SCO development due to failure of the closure of the cerebral aqueduct⁷. Mutant hydrocephalus with hop gait (hyh) mice develop postnatal hydrocephalus with absence of the central canal in the spinal cord and stenosis of the cerebral aqueduct⁸. Further studies with hyh mice revealed impairment of both the SCO and formation of the Reissner fiber (RF)^{9,10}. The RF is an insoluble filament formed mainly by SCO-secreted glycoproteins called SCO-spondins¹⁰.

However, there has been no agreement on SCO or RF function. The lack of the RF in hyh mice may cause distortion and collapse of the ependyma¹¹. In zebrafish, the RF participates in spine morphogenesis¹², and its dysfunction leads to scoliosis phenotypes¹³. The RF in zebrafish was observed to contribute to the mechanosensitivity of neurons that contact the cerebrospinal fluid (CSF)¹⁴.

In addition to the correlation between SCO malformation and congenital hydrocephalus and scoliosis, it has been proposed to be involved in sodium excretion, diuresis, osmoregulation and water intake in the brain^{9,10,15}, although these findings remain controversial^{10,16}. During early brain development in vertebrates, the SCO and its secreted proteins help facilitate axonal guidance in the neural tube midline^{17,18}, the regeneration of the neural tube after injury¹⁷ and the modulation of neuronal aggregation¹⁹. In addition, soluble factors secreted by the SCO may contribute to neurogenesis in adult mammals³. However, most of the information concerning SCO function

A full list of affiliations appears at the end of the paper.  e-mail: lingjun.li@wisc.edu; sunwenzhi@cibr.ac.cn; woopingge@cibr.ac.cn

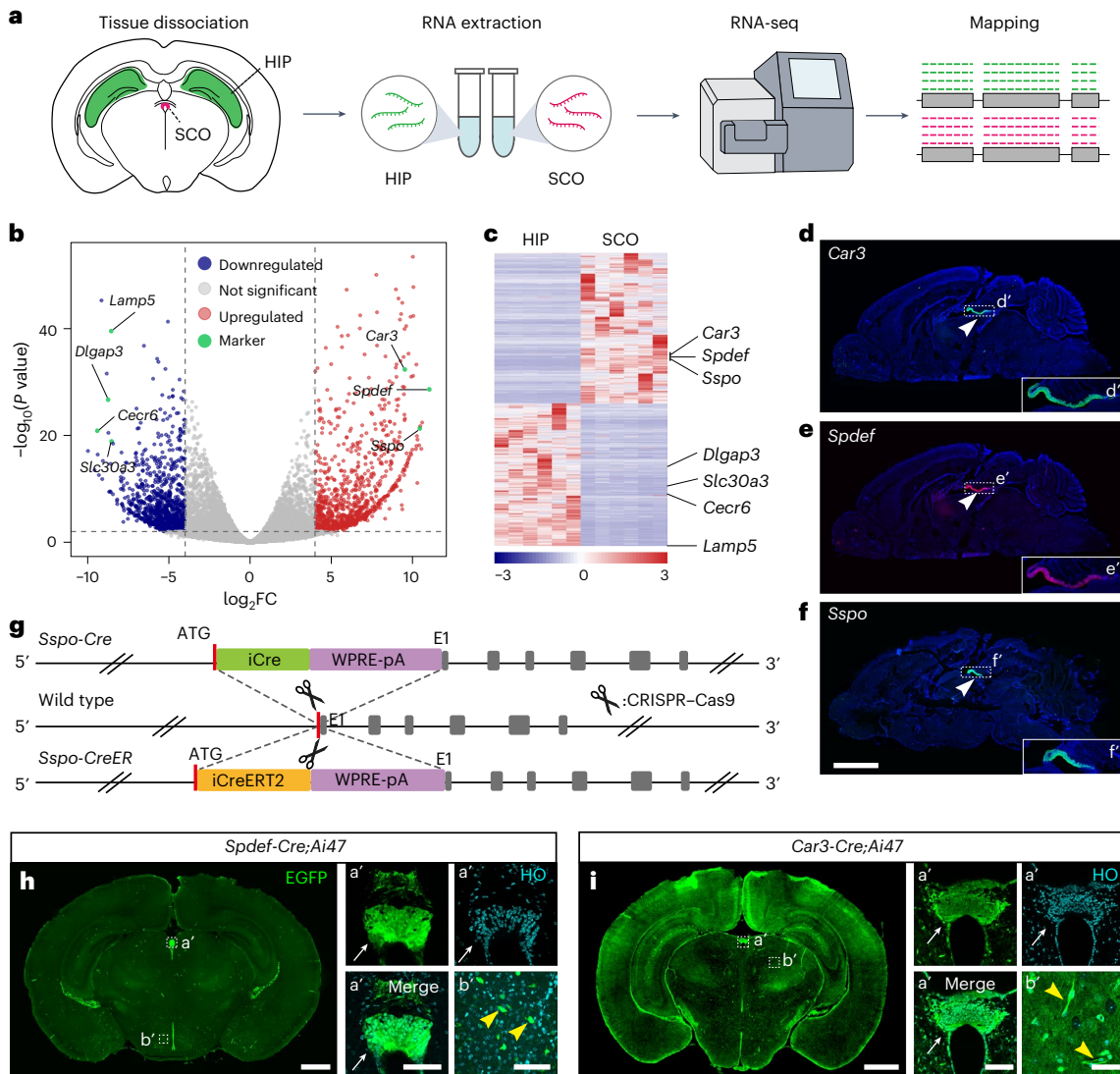


Fig. 1 | Identifying genes expressed specifically in SCO cells and developing corresponding Cre/CreER mouse lines. **a**, Strategy for screening genes for which expression was enriched in SCO cells compared with cells from the hippocampus (HIP). The SCO and HIP of adult mice (postnatal days 56–70) were excised for bulk RNA-seq and analysis. **b, c**, Analysis of differentially expressed genes (upregulated or downregulated) in each of the SCO and HIP, presented as volcano plot (**b**) and clustered heatmap (**c**). *Sspo*, *Spdef* and *Car3* were among the most highly specifically upregulated genes identified in the SCO. *Dlgap3*, *Slc30a3*, *Cecr6* and *Lamp5* were four representative genes significantly upregulated in the HIP but downregulated in the SCO. The scale indicates the fold change (FC) and the expression level. **d–f**, Fluorescence imaging of

mRNAs transcribed from *Car3* (**d**), *Spdef* (**e**) and *Sspo* (**f**) as determined with RNAscope mFISH of the adult mouse brain. Green, pseudocolor of Opal 520; red, pseudocolor of Opal 570; blue, nuclei stained by Hoechst 33342 (HO). The arrowheads in **d–f** indicate the boxed areas enlarged in insets **d'–f'**. The images in **d** and **e** are from the same brain section stained with two probes. **g**, Strategy for generating mouse strains *Sspo-Cre* and *Sspo-CreER*. **h, i**, EGFP expression profiles for cells in the brain of *Spdef-Cre;Ai47* (**h**) and *Car3-Cre;Ai47* mice (**i**). Green, cells expressing EGFP; light blue, nuclei labeled by Hoechst 33342 (HO). Arrows in **h**, SCO; yellow arrowheads in **h**, neurons in the hypothalamus; white arrows in **i**, SCO; yellow arrowheads in **i**, blood vessels. **a'** and **b'** are insets. Scale bars, 2 mm (**d–f**), 1 mm (**h** and **i**) and 100 μ m (**h** inset **a'**, **h** inset **b'**, **i** inset **a'** and **i** inset **b'**).

has come from cell culture experiments or SCO xenografting and isografting models^{20,21}.

The conventional approach to studying the function of a particular brain region is to surgically lesion the area, for example, by electrolysis²². However, the SCO is a tiny gland in the central brain located at the entrance of the aqueduct of Sylvius¹⁰, making it exceptionally challenging to create lesions without affecting cells in neighboring brain regions. Fortunately, however, genetic ablation via Cre recombinase-mediated expression of diphtheria toxin fragment A (DTA) in targeted cells represents an efficient and specific way to evaluate the function of a group of cells in the body with minimal impact on adjacent cells²³. In this article, using this approach to compare the transcriptome of mouse SCO with that of non-SCO brain regions,

we were able to identify three genes (*Spdef*, *Car3* and *Sspo*) that are highly expressed in the SCO. Using the promoters for these genes, we developed three Cre mouse strains (*Spdef-Cre*, *Car3-Cre* and *Sspo-Cre*) and one CreER strain (*Sspo-CreER*) for studies of SCO development and function.

Results

Generation of SCO-specific Cre mouse lines

We carried out a transcriptomic analysis of the SCO (and hippocampus, for comparison; Fig. 1a) to identify genes that are expressed specifically in the SCO; this analysis yielded >200 genes that were highly expressed specifically in the SCO (Fig. 1b,c). The relative levels of the messenger RNAs expressed at the whole-brain level were

analyzed using an in situ hybridization (ISH) dataset from the Allen Mouse Brain Atlas, aiming to narrow the number of candidate genes that showed specific SCO labeling. We identified three genes, namely *Sspo*, *Car3* and *Spdef*, that were expressed in the SCO and that met our four criteria: (1) mRNA abundance was among the top 10% of all mRNAs expressed in the SCO, (2) the *P* value was among the top 200 when compared with hippocampal mRNAs, (3) the fold change (upregulated) relative to hippocampal mRNAs was among the top 100 and (4) the ISH results from our RNAscope multicolor fluorescence in situ hybridization (mFISH) analysis were verified by comparison with ISH data from the Allen Institute ISH database. Strong signals for the corresponding probes of these three candidate genes were limited to the SCO region, implicating their specificity for SCO cells (Fig. 1d–f and Supplementary Fig. 1).

To further assess SCO-specific gene expression and evaluate SCO function, we generated three Cre transgenic mouse lines: *Car3-Cre*, *Spdef-Cre* and *Sspo-Cre* (Fig. 1g and Supplementary Fig. 2a). To manipulate gene expression in the SCO from mice at different developmental stages, we also generated mouse line *Sspo-CreER* (Fig. 1g). For each line, a part of the sequence of the corresponding gene was replaced with Cre; thus, the expression level and profile of Cre reflected that of the inserted gene. To evaluate the specificity of these mouse lines, mice were crossed with one of two reporter mouse lines, namely *Ai47* (LSL-Rosa-EGFP) or *Ai14* (LSL-Rosa-tdTomato)^{24,25}. SCO cells were labeled with EGFP in *Spdef-Cre;Ai47* mice, whereas only a small percentage of neurons were labeled (Fig. 1h). *Car3-Cre;Ai47* mice could also be used for SCO labeling, but some blood vessels expressed EGFP (Fig. 1i). We observed not only SCO cells but also some choroid-plexus cells and ependymal cells labeled in both *Spdef-Cre;Ai47* and *Car3-Cre;Ai47* mice (Supplementary Fig. 2b). After crossing *Sspo-CreER* mice with *Ai47* mice to induce Cre-dependent EGFP expression in *Sspo*-expressing cells via administration of tamoxifen during embryonic to adolescent stages, *Sspo* was expressed only in SCO cells from the embryonic stage (Fig. 2a,b,f and Supplementary Fig. 3) to adolescent stage (Fig. 2c–e). In addition, no Cre was expressed in the spinal cord. In *Sspo-Cre;Ai47* mice (Fig. 2g), EGFP also was highly expressed in the SCO. We further stained brain sections from *Sspo-Cre;Ai47* and *Sspo-CreER;Ai47* mice with an antibody specific for Foxj1, S100 β or β -catenin for labeling ependymal cells or choroid-plexus cells (Fig. 2f,i and Supplementary Figs. 3 and 4). No EGFP⁺ ependymal or choroid-plexus cells were detected in brain sections of *Sspo-CreER;Ai47* mice (Fig. 2f and Supplementary Fig. 3). In *Sspo-Cre;Ai47* mice, only 0.09% of the ependymal cells and 0.33% of the choroid-plexus cells were EGFP⁺ (Fig. 2h,i and Supplementary Fig. 4). However, EGFP⁺ cells were not detected in ependyma around the third and fourth ventricles or central canal (Supplementary Figs. 3 and 4). SCO-spondin has been reported to be expressed in this area in some species²⁶; however, no green fluorescence was detected in the floor plate of *Sspo-Cre;Ai47* mice (embryonic day (E)12–18) (Supplementary Fig. 5). These results indicated that mouse lines *Sspo-Cre* and *Sspo-CreER* were ideal for SCO genetic manipulation.

The mouse SCO is first recognizable on embryonic day E10–11 (ref. 27), but it is unclear how the number of SCO cells changes during brain development. Therefore, we counted SCO cells at different embryonic and postnatal stages on the basis of Hoechst 33342 staining and EGFP expression in wild-type and *Sspo-Cre;Ai47* mice (Fig. 2j and Supplementary Fig. 6). After postnatal day (P)5, the number of SCO cells decreased to ~6,000 and remained relatively small thereafter, with no gender difference (Fig. 2k,l). For *Sspo-Cre;Ai47* mice at different developmental stages, 86–99% of SCO cells were EGFP⁺ (Fig. 2m). Further, use of *Sspo-CreER;Ai47* mice to sparsely label SCO cells with a relatively lower dosage of tamoxifen revealed that most EGFP⁺ cells sent their processes to the third ventricle and were in contact with CSF (Supplementary Fig. 7). This indicated that most SCO cells were specialized ependymal cells.

Genetic ablation of SCO cells leads to brain abnormalities

To study SCO function in the brain, the SCO was subjected to genetic ablation by crossing *Sspo-Cre* or *Sspo-CreER* mice with Cre-dependent *DTA* mice. Cre was expressed only in SCO cells of *Sspo-CreER* and *Sspo-Cre* mice (Fig. 2). In *Sspo-Cre;DTA* mice, the SCO was experimentally ablated from E11 to E12. In *Sspo-CreER;DTA* mice, ablation was performed at different developmental stages depending on the time of tamoxifen injection. As a result, *Sspo-CreER;DTA* and *Sspo-Cre;DTA* mice could be used to evaluate the role of the SCO with or without tamoxifen application, respectively (Fig. 3a), enabling targeted SCO ablation in mice at different embryonic or postnatal stages. We did not detect a difference in cortical layer structures, cortical cell density and body weight between the wild-type and *Sspo-Cre/Sspo-CreER* heterozygous mice (Supplementary Fig. 8), and thus, these mice were used as the control. However, *Sspo-Cre;DTA* mice were significantly smaller than wild-type mice (Fig. 3b,c). Overall survival of *Sspo-Cre;DTA* mice dropped dramatically from P8, and ~80% of mice died before P24 (Fig. 3d). Furthermore, *Sspo-Cre;DTA* mice that underwent SCO ablation had a bulged head and enlarged brain (Fig. 3e–g). Labeling of cellular nuclei with Hoechst 33342 revealed notable enlargement of the lateral ventricles in *Sspo-Cre;DTA* mice (Fig. 3h,i), and nearly all SCO cells were lost by P22 (Fig. 3h,i). Furthermore, SCO-spondin was present in CSF of control neonatal pups (P0–P3) but absent in CSF of *Sspo-Cre;DTA* mice. Moreover, RF was detectable in the central canal of *Sspo-Cre* mice but was absent in *Sspo-Cre;DTA* mice. These results documented that the SCO was ablated in *Sspo-Cre;DTA* mice (Supplementary Figs. 9 and 10 and Supplementary Table 1). To further understand how SCO ablation caused brain developmental abnormalities, magnetic resonance imaging (MRI) was carried out with *Sspo-Cre;DTA* mice at several postnatal stages. These mice exhibited clear progression of hydrocephalus with significant enlargement of ventricles (Fig. 3j–l). We used anti-S100 β to stain ependymal cells and anti- β -catenin to stain choroid-plexus cells in control and *Sspo-Cre;DTA* mice (P0 and P12), revealing no differences in cell density or morphology of ependyma and choroid plexus, and the ependymal cells in the aqueduct and central canal of *Sspo-Cre;DTA* mice were well aligned, were cilia-rich and possessed complete cellular structures (Supplementary Figs. 11 and 12). Moreover, there were no apparent differences in the ventricular foramina, cerebral (Sylvian) aqueduct or central canal between wild-type and *Sspo-Cre;DTA* mice at P0, P3, P6 or P12 (Supplementary Fig. 13). Therefore, the hydrocephalus defects after SCO ablation were possibly noncommunicating.

The brain of the *Sspo-Cre;DTA* mice was malformed at P3 (Fig. 3m). To determine whether the SCO contributes to embryonic brain development, we induced *Sspo-CreER;DTA* mice with tamoxifen from E10 and observed similarly expanded ventricles at P3 (Fig. 3n), indicating that the SCO contributes to fetal brain development. Initiation of SCO ablation at P3 and brain collection at P37 revealed a slight expansion of the third ventricle (Supplementary Fig. 14). However, when SCO ablation was initiated at P25 and brains collected at P70, we did not observe an apparent ventricular expansion in the brain (Supplementary Fig. 14). Further, there were no apparent differences in neuronal density, distribution or morphology in the cerebral cortex (Supplementary Figs. 15 and 16). These results suggested that the SCO plays a critical role in early brain development.

SCO contributes to neuronal development in vivo

Studies with chicken embryos have shown that the SCO promotes both neuronal adhesion and neurite growth in vitro^{21,28}. To determine how SCO ablation would alter neuronal development in mice, neurons or neuronal progenitors were stained with an antibody against NeuN, SATB2, CTIP2 or TBR1 in *Sspo-Cre;DTA* mice (Fig. 4a–j). In the P3 brain, cortical neuron loss was slight (Fig. 4a,b), whereas loss was much greater at P22, at which time the six cortical layers could not

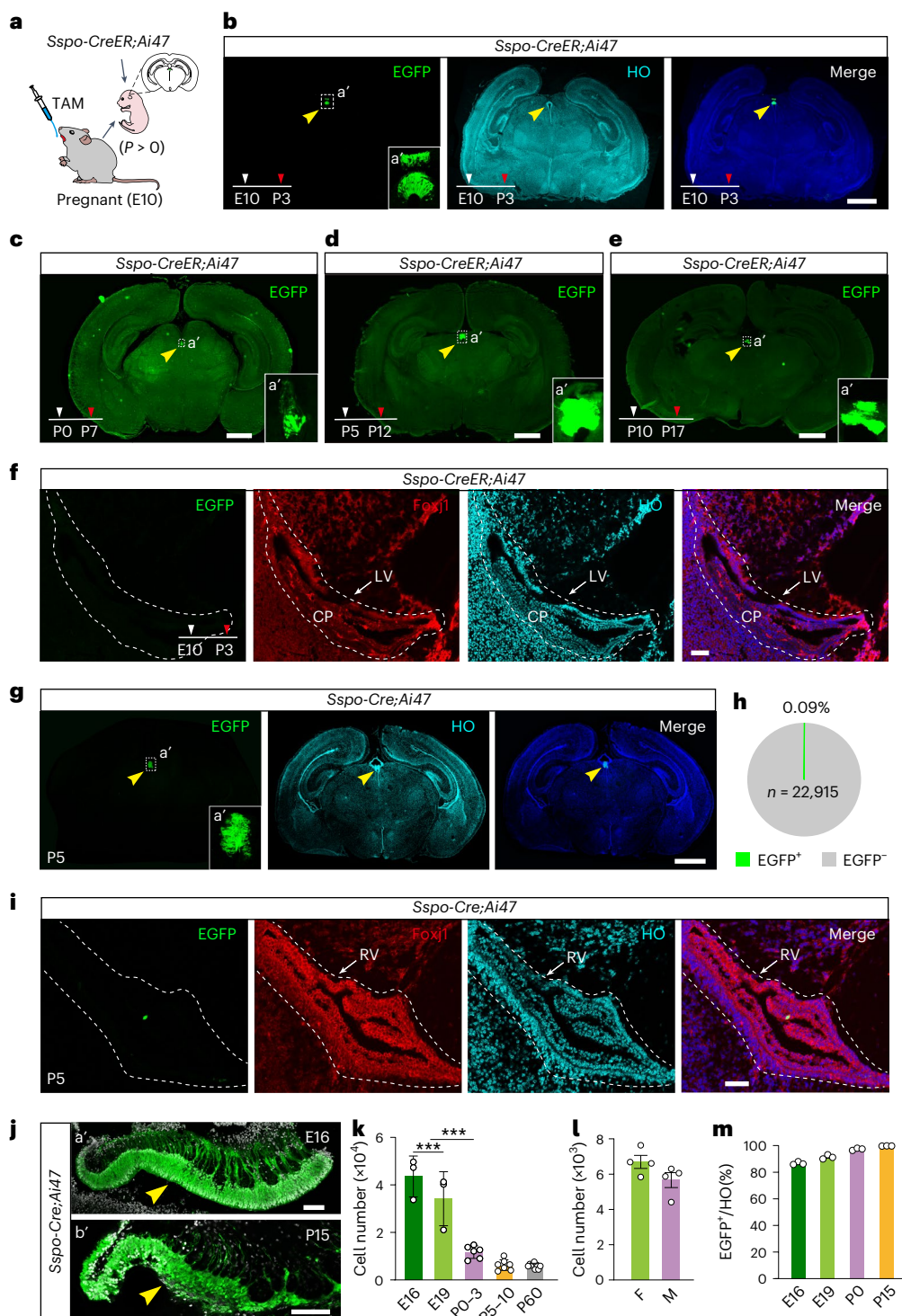


Fig. 2 | Specificity of *Sspo-CreER* and *Sspo-Cre* mouse strains for SCO labeling.

a, The procedure for administering tamoxifen (TAM) to E10 *Sspo-CreER;Ai47* mice. **b–e**, EGFP expression profiles from the brain of *Sspo-CreER;Ai47* mice after tamoxifen was administered at E10 (**b**), P0 (**c**), P5 (**d**) and P10 (**e**); brains were collected at P3 (**b**), P7 (**c**), P12 (**d**) and P17 (**e**), respectively. Yellow arrowheads, SCO; a', inset. **f**, Image of the lateral ventricle from the brain of a *Sspo-CreER;Ai47* mouse at P3 after tamoxifen was administered at E10. Green, EGFP; red, ependymal cells stained with anti-Foxj1. LV, lateral ventricle; CP, choroid plexus. The dashed lines indicate the LV margin. **g**, EGFP expression in the brain of a *Sspo-Cre;Ai47* mouse at P5. Green, EGFP; yellow arrowheads, SCO. a', inset. **h**, The percentage of ependymal cells with EGFP fluorescence in *Sspo-Cre;Ai47* mice at P5 ($n = 22,915$ ependymal cells in total). **i**, Images of LV from the brain of a *Sspo-Cre;Ai47* mouse at P5. Green, EGFP fluorescence; red, ependymal cells stained

with anti-Foxj1. The dashed lines indicate the LV margin. **j**, The morphology of SCO in sagittal brain sections of *Sspo-Cre;Ai47* mice at E16 (a') and P15 (b'). Green, EGFP; white, nuclei stained by Hoechst 33342 (HO); yellow arrowheads, SCO.

k, The number of SCO cells in mice of different ages ($n = 3–8$ per group) (E16 and E19, $n = 3$ mice per group; P0–3, $n = 6$ mice; P5–10, $n = 7$ mice; P60, $n = 8$ mice). **l**, The number of SCO cells in the brain of adult male (M) and female (F) mice ($n = 4$ mice per group). **m**, The percentage of SCO cells exhibiting EGFP fluorescence in *Sspo-Cre;Ai47* mice (E16–P15, $n = 3$ mice per group). Scale bars, 1 mm (**b–e** and **g**), 100 μm (**j** inset b') and 50 μm (**f**, **i** and **j** inset a'). Two-tailed unpaired *t*-test, $***P < 0.001$. Error bars, s.e.m. White arrowheads, the starting point of tamoxifen injection; red arrowheads, time points for mouse killing (**b–f**); green, EGFP fluorescence (**b–j**); light blue, blue or white, nuclei stained by Hoechst 33342 (HO; **b**, **f**, **g**, **i** and **j**).

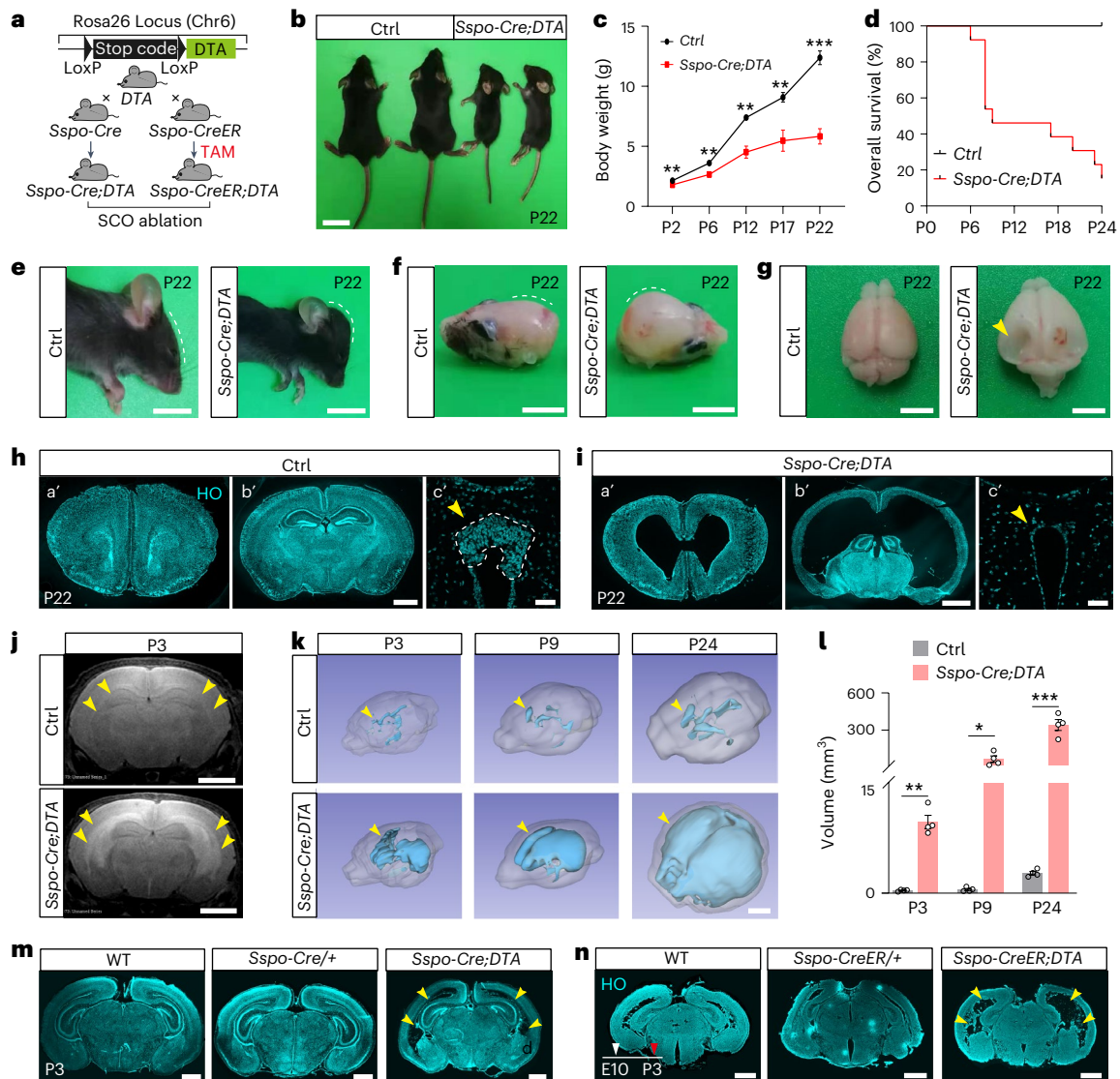


Fig. 3 | Phenotypes observed in SCO-ablated mice. a, The breeding strategy for *Sspo-Cre;DTA* and *Sspo-CreER;DTA* mice. **b**, Images of wild-type (Ctrl, P22, left) and *Sspo-Cre;DTA* mice (P22, right). **c**, The body weight of *Sspo-Cre;DTA* (red) and control mice (black) at P2, P6, P12, P17 and P22. $n = 9$ (P2), 9 (P6), 7 (P12), 6 (P17), 5 (P22, *Sspo-Cre;DTA*) and 6 (P22, Ctrl). **d**, The overall survival of *Sspo-Cre;DTA* mice (red, $n = 13$) and control mice (black, $n = 13$). **e–g**, Images of the head (**e**), skull (**f**) and brain (**g**) of *Sspo-Cre;DTA* and control mice at P22. Dashed lines, skull curvature; arrowhead, collapsed cerebral cortex in the brain of a *Sspo-Cre;DTA* mouse. **h**, Images of coronal brain sections (**a'** and **b'**, different locations) from control mice at P22. Dashed line (**c'**), SCO margin; yellow arrowheads (**c'**), location of the SCO; light blue, nuclei stained with Hoechst 33342 (HO). **i**, Images of brain sections (**a'** and **b'**) from *Sspo-Cre;DTA* mice at P22. Yellow arrowhead (**c'**), location of ablated SCO; light blue, nuclei stained with Hoechst 33342 (HO).

j, k, Representative MRI images (**j**, P3) and 3D reconstructed images (**k**, P3, P9 and P24) of *Sspo-Cre;DTA* and control mice. Yellow arrowheads (**j** and **k**), lateral ventricle; translucent white, 3D outline of the whole brain; blue, 3D outline of the lateral and third ventricles. **l**, Volumes of ventricles in control (Ctrl) and *Sspo-Cre;DTA* mice at P3, P9 and P24 ($n = 4$ mice per group). **m, n**, Representative coronal brain sections of *Sspo-Cre;DTA* (**m**) and *Sspo-CreER;DTA* (**n**) mice and corresponding controls. Tamoxifen (TAM) was administered at E10, and mice were killed at P3. WT, wild type; light blue, nuclei stained by Hoechst 33342 (HO); yellow arrowheads, lateral ventricles; white arrowhead, the starting point of tamoxifen injection; red arrowhead, the time point for mouse killing. Scale bars, 1 cm (**b**), 5 mm (**e–g**), 2 mm (**j** and **k**), 1 mm (**h** insets **a'** and **b'**, **m** and **n**) and 50 μ m (**h** inset **c'** and **i** inset **c'**). Two-tailed unpaired *t*-test, * $P < 0.05$, ** $P < 0.01$, *** $P < 0.001$. Error bars, s.e.m.

be easily distinguished (Fig. 4c,d). Further, neuronal death increased significantly in the P3 brain but less so at P8 (Supplementary Fig. 17). Therefore, after SCO ablation, cortical neurons were gradually lost postnatally. Furthermore, the cortex was thinner at E18, when hydrocephalus had yet to manifest (Supplementary Fig. 18). Antibodies also were used for labeling neurons in different layers of the cerebral cortex of *Sspo-Cre;DTA* mice. These antibodies included SATB2 (layers II–VI; Fig. 4e–g), CTIP2 (layers V–VI; Supplementary Fig. 18) and TBR1 (layer VI; Fig. 4h–j). The numbers of SATB2⁺, TBR1⁺ and CTIP2⁺ neurons were significantly reduced in the cerebral cortex at E18 (Fig. 4e–j and Supplementary Fig. 18) and P22 (Supplementary Fig. 19).

Next, we injected pregnant *Sspo-Cre;DTA* mice once with 5-ethynyl-2'-deoxyuridine (EdU) at E15 and collected each pup brain at E18 for staining (Fig. 4k–n). The number of EdU⁺ cells in the cerebral cortex decreased dramatically (Fig. 4k–m). Further, the percentage of EdU⁺ cells was lower in both the superficial and deeper layers compared with wild-type mice (Fig. 4k,l,n). Finally, some NeuN⁺ neurons appeared in the white matter between layer VI and the subventricular zone of P3 mice (Supplementary Fig. 20). This observation indicated that a portion of neurons generated from the subventricular zone might not have successfully migrated to the appropriate cortical layer(s) during embryonic stages and more neurons underwent apoptosis postnatally

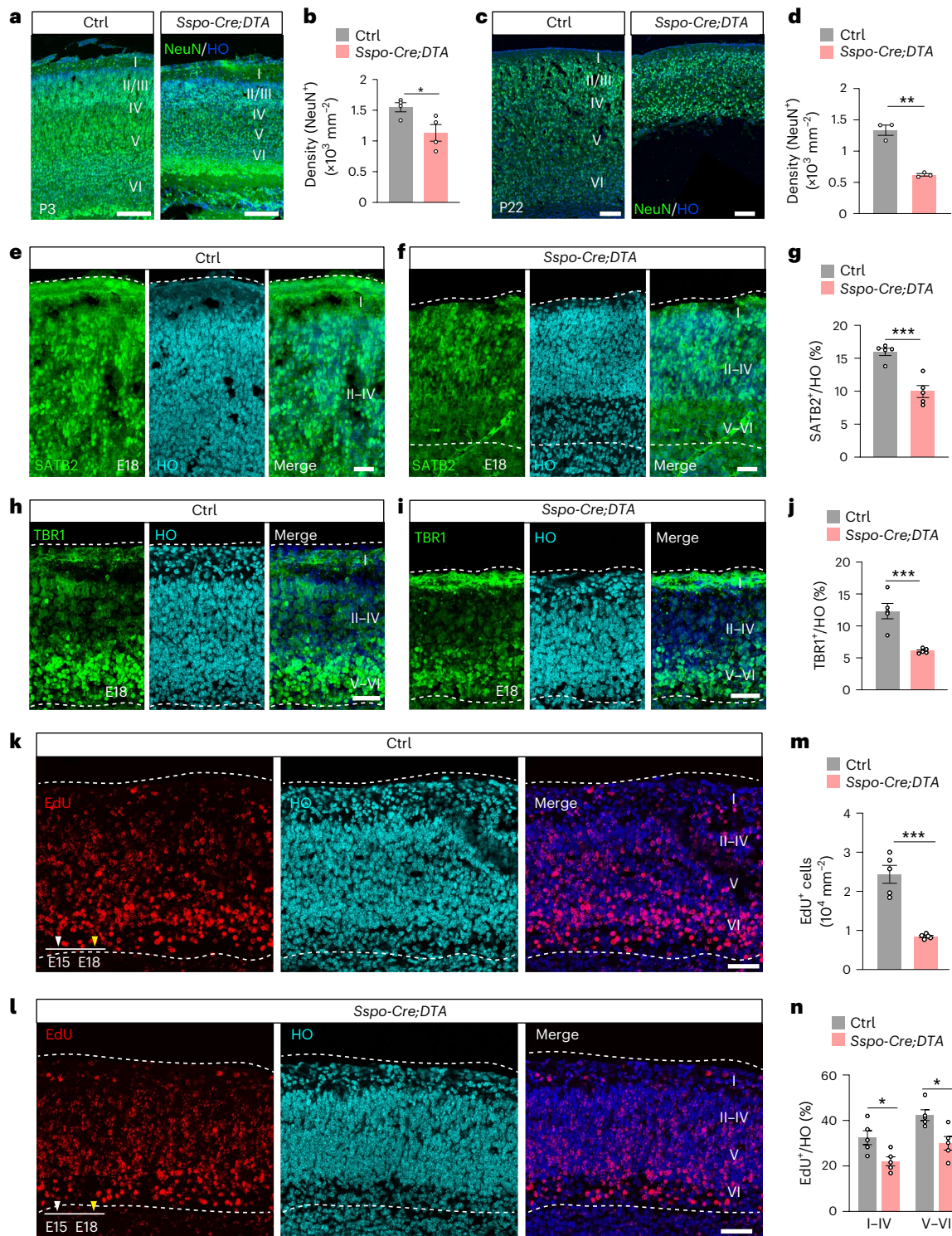


Fig. 4 | Neuronal properties of the mouse brain after SCO ablation.

a–d, Images of coronal brain sections and density of NeuN⁺ cells from the cerebral cortex of *Sspo-Cre;DTA* and control mice at P3 (**a**, **b**, $n = 4$ regions per group) and P22 (**c**, **d**, $n = 3$ regions per group). Green, neurons stained with anti-NeuN. **e, f**, Images of coronal sections from the cerebral cortex of *Sspo-Cre;DTA* (**f**) and control mice (**e**) at E18. Green, neurons stained with anti-SATB2. **g**, The percentage of SATB2⁺ cells among total cells in the whole cerebral cortex from *Sspo-Cre;DTA* and control mice at E18 ($n = 5$ regions per group). **h, i**, Images of coronal sections from the cerebral cortex of *Sspo-Cre;DTA* and control mice at E18. Green, neurons stained with anti-TBRI1. **j**, The percentage of TBRI1⁺ cells among total cells in the whole cerebral cortex from *Sspo-Cre;DTA* and control

mice at E18 ($n = 5$ regions per group). **k, l**, Images of coronal sections from the cerebral cortex of *Sspo-Cre;DTA* and control mice at E18. Red, cells stained with EdU. **m**, The density of EdU⁺ cells in the cerebral cortex of *Sspo-Cre;DTA* and control mice at E18 ($n = 5$ regions per group). **n**, The percentage of EdU⁺ cells among total cells of cortical layers I–V and V–VI from *Sspo-Cre;DTA* and control mice at E18 ($n = 5$ regions per group). Scale bars, 200 μm (**a**), 100 μm (**c**), 50 μm (**e**, **f**, **h**, **i**, **k** and **l**). Two-tailed unpaired *t*-test, * $P < 0.05$, ** $P < 0.01$, *** $P < 0.001$. Error bars, s.e.m. Light blue or blue (**a**, **c**, **e**, **f**, **h**, **i**, **k** and **l**), nuclei stained with Hoechst 33342 (HO); I–VI (**a**, **c**, **e**, **f**, **h**, **i**, **k** and **l**), six layers of the cerebral cortex; white arrowheads (**k** and **l**), the time point of EdU injection; yellow arrowheads (**k** and **l**), the time point of mouse killing; dashed lines (**e**, **f**, **h**, **i**, **k** and **l**), cortical margin.

in *Sspo-Cre;DTA* mice, which is consistent with the reduced number of neurons at P3. These results implied that neuronal properties may have been altered before hydrocephalus onset although hydrocephalus might have caused neuronal death in later developmental stages.

SCO contributes to neuronal development and survival

To further examine the contribution of the SCO to neuronal development, neurons in transwells were co-cultured with a resected SCO (SCO^W) or hippocampal tissue (Hip) or cultured alone (SCO^{W/O}) (Fig. 5a). Neuronal density in the SCO^W, Hip and SCO^{W/O} groups was comparable before day 6 in vitro (DIV6) but then gradually decreased in the SCO^{W/O} and Hip groups. At DIV13, the density was significantly greater in the SCO^W group, indicating the SCO could maintain neuronal survival (Fig. 5b,c). This result was consistent with observations made in the cortex of *Sspo-Cre;DTA* mice (Fig. 5i–q). Incubation of neurons with anti-Tuj1 (neurite marker) revealed reduced complexity of neurites of the SCO^{W/O} and Hip groups (Fig. 5d). To evaluate neuronal morphology in vitro, neurons were infected with lentivirus (LV)-HI-EGFP (Fig. 5e). The number of neurites (including dendrites and axons) was approximately doubled in the SCO^W group (Fig. 5f–h), suggesting that the SCO promotes neurite growth.

Previous results from SCO co-culturing and grafting studies have established that the SCO promotes neuronal development^{20,21}, but the impact of SCO ablation on neuronal development in vivo remains largely unknown. To address this issue, a low dose of adeno-associated virus (AAV)-CAG-EGFP was injected into the lateral ventricle of *Sspo-Cre;DTA* mice as well as controls (*DTA*, *Sspo-Cre* and wild type) at E15–18. Neuronal morphology in the cerebral cortex was then assessed (Fig. 5i). At P5, the *Sspo-Cre;DTA* brain had a high percentage of cortical neurons with abnormally polarized axons and apical dendrites (Fig. 5j–l). A three-dimensional (3D) reconstruction revealed that apical dendrites were shorter in *Sspo-Cre;DTA* mice (Fig. 5n,o). *Sspo-Cre;DTA* neurons also had fewer branches, with abnormally polarized axons (Fig. 5m,n,p,q). We further stained brain sections with anti-EGFP to observe spines in dendrites and boutons in axons to establish neuron polarity in the cerebral cortex. Neurons indeed had inverted polarity in *Sspo-Cre;DTA* mice (Fig. 5k). These results demonstrated that the SCO promotes neuronal survival and development both in vitro and in vivo.

Peptides secreted by SCO promote neuronal development

To elucidate the molecular mechanism underlying SCO regulation of neuronal development, RNA sequencing (RNA-seq) and mass spectrometry (MS)-based peptidomics were carried out to assess the involvement of SCO-derived secretory molecules. EGFP⁺ SCO cells in the brain of *Sspo-CreER;Ai47* mice sent processes to the third ventricle (Fig. 6a and Supplementary Fig. 7). Golgi were abundant in SCO cells adjacent to the third ventricle (Fig. 6a), indicating that SCO cells are highly secretory cells. Transcriptome analysis of each of SCO and hippocampus revealed that the positive regulation of peptide-hormone secretion pathway was highly enriched in the SCO (Fig. 6b and Supplementary Fig. 21). We thus searched for SCO peptides that might contribute to neuronal development. A systems-level peptidomic analysis of SCOs from 120 mouse brains and corresponding hippocampal tissue (Fig. 6c) identified 2,788 (hippocampus) and 3,588 (SCO) de novo peptide-associated features (Fig. 6d,e). Interestingly, the vast majority (~92%) of features found in SCO samples were unknown compared with only ~12% for the hippocampus (Fig. 6d,e). The SCO features were further searched using the peptide databases Neurop and SwePep, resulting in the annotation of 12 mature peptides that were highly enriched in the SCO (Supplementary Table 2). Of these, nine peptides exhibited 100% sequence coverage, including manserin (Fig. 6f), which regulates neuroendocrine pathways. To our knowledge, this peptide has not previously been identified in mice. The preprohormones of these 12 peptides belong to a variety of subfamilies, including the thymosin beta (Tβ), granin (chromogranin/secretogranin),

melanin-concentrating hormone, opioid and somatostatin families (Fig. 6g). Among these, the Tβ family is related to embryonic development^{29,30}. Moreover, Tβ10 and Tβ4 showed unique post-translation modifications and glycosylation, with one O-glycosylated peptide from Tβ10 and eight from Tβ4. Comparison with glycosylated peptides identified in the hippocampus (control) sample revealed four O-glycosylated peptides from Tβ4 that were specific to the SCO. Therefore, we selected Tβ4 and Tβ10 for further investigation along with a previously unidentified bioactive 24-residue peptide that we named NP24 (DVGSYQEKVDVVLGPIQLQSPSKE), detected with high cleavage probability ($P = 0.9906$) in the SCO group.

Next, we collected and pooled CSF from 20–30 wild-type or *Sspo-Cre;DTA* perinatal mice (E18–P0); peptides Tβ4, Tβ10 and NP24 were detected in wild-type CSF (Supplementary Fig. 22). The concentrations of Tβ4 and Tβ10 were substantially lower in CSF from *Sspo-Cre;DTA* mice (Fig. 6h and Supplementary Table 3). Notably, the concentration of five different Tβ4 segments was only 0–13% of that measured in wild-type CSF, and the concentration of Tβ10 was only 0–4% that of wild type. NP24 was not detected in CSF from *Sspo-Cre;DTA* mice. These results demonstrated that SCO is the main source of these three peptides in CSF. Indeed, the results indicated a potential additional source of Tβ4 and Tβ10 in the CSF of brain and that nearly all NP24 is derived from SCO.

The potential roles of these three SCO peptides in neuronal development were examined by applying Tβ4, Tβ10 and NP24 to primary cultured neurons, which significantly increased neuron density and prolonged their survival (Fig. 7a,b and Supplementary Fig. 23). In addition, the peptide-treated neurons had more complex morphology, with longer processes and more branches and terminal points (Fig. 7c–e and Supplementary Fig. 23). Finally, RNA-seq of neurons incubated for 2 days with these peptides revealed that they promoted neuronal development via activation of specific pathways (Supplementary Fig. 24).

To test whether application of the Tβ4–Tβ10–NP24 cocktail could rescue the phenotype of *Sspo-Cre;DTA* mice, the cocktail was injected into the lateral ventricle of mice once every 3 days from P0 (3 μg each time). The cocktail-treated mice survived significantly longer than did the saline-treated *Sspo-Cre;DTA* mice at P24 (overall survival 75% versus 33.3%, respectively; Fig. 8a), and they also attained a higher mean body weight (Fig. 8b). MRI revealed that the cocktail-treated mice exhibited less severe ventricle expansion and reduced hydrocephalus (Fig. 8c,d), which was verified through staining cell nuclei in coronal brain sections (Fig. 8e,f). Notably, the ventricular area in the cocktail-treated mice was reduced by ~60% compared with saline-treated controls (Fig. 8g). Further, the percentage of neurons with abnormally polarized axons and shorter dendrites was vastly reduced in cocktail-treated mice (Fig. 8h–j). These results indicated that SCO-secreted peptides might contribute to neuronal development and help mitigate abnormalities in SCO-ablated mice. We applied individual peptides (at two different concentrations) to the brain of *Sspo-Cre;DTA* mice for rescue tests; each of the three peptides could also partially rescue the phenotype observed in SCO-ablated mice including longer survival (Fig. 8k–m) and reduced ventricular volume (Fig. 8n–q). However, no individual peptide could fully rescue the phenotype, indicating that other peptides or proteins from SCO might also contribute to rescuing the *Sspo-Cre;DTA* phenotype.

Discussion

The genetic mouse models we developed make it possible to ablate cells specifically in the SCO and, thus, address its function in the brain. Our findings suggest that SCO cells are de facto secretory cells, and indeed we identified three SCO-secreted peptides, namely Tβ4, Tβ10 and a new peptide NP24, that contribute to neurite development and neuronal survival in vitro.

SCO cells are bipolar: their apical poles face the third ventricle, whereas their basal processes face the subarachnoid space and contact

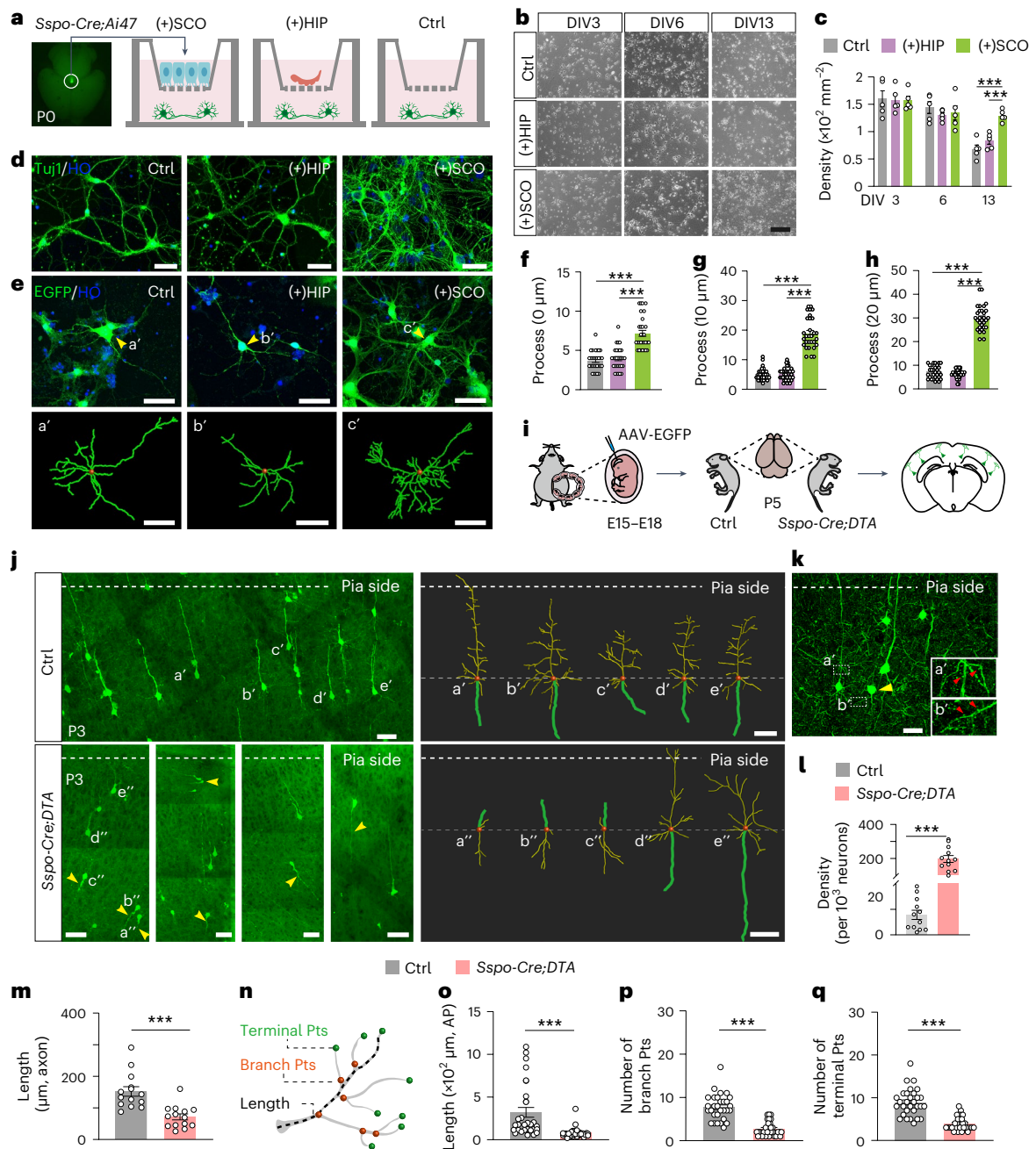


Fig. 5 | SCO promotes neuronal development. **a**, Strategy for culturing neurons in the absence or presence of the SCO. The SCO was resected from *Sspo-Cre;Ai47* pups. HIP, hippocampus. **b, c**, Images and density of neurons co-cultured with SCO (bottom), hippocampus (middle, HIP) or alone (top) at DIV3, 6 and 13 ($n = 5$ wells per group). **d, e**, The morphology of neurons. Green, neurons stained with anti-Tuj1 (**d**) or EGFP in neurons infected by LV-H1-EGFP (**e**); blue, Hoechst 33342 (HO, nuclei). **a'–c'** show the morphology of three representative neurons in three groups: Ctrl (**a'**), co-cultured with hippocampus (**b'**) or co-cultured with SCO (**c'**). **f–h**, The number of neurites after LV-H1-EGFP injection, located at the soma (**f**, 0 μm) or 10 μm (**g**) or 20 μm away from the soma (**h**). $n = 25$ neurons per group. **i**, Procedure for sparse neuronal labeling. AAV-CAG-EGFP was injected at E15–18, and the brains were collected at P5. **j**, The morphology of neurons in the brain of *Sspo-Cre;DTA* and control mice. **a'–e'** show representative neurons in control mice. **a''–e''** show abnormal neurons with apical dendrites directed toward the corpus callosum and axons facing the pial surface in *Sspo-Cre;DTA*

mice; **d''** and **e''** show neurons with apical dendrites directed toward the pial surface and axons facing the corpus callosum in *Sspo-Cre;DTA* mice; arrowheads, neurons with abnormal polarity; soma, red; axons, green; dendrites, yellow. **k**, The morphology of sparsely labeled neurons in the brain of a *Sspo-Cre;DTA* mouse. Green, anti-GFP; yellow arrowheads, neurons with abnormal polarity; red arrowheads, spines of a neuron with normal (**a'**) or abnormal (**b'**) polarity. **l, m**, The density of neurons with apical dendrites facing the side of the corpus callosum ($n = 12$ regions per group) and the length of axons ($n = 14$ neurons per group) in *Sspo-Cre;DTA* and control mice at P5. **n–q**, Analysis of apical dendrites at P5 including the length of apical dendrites (**n**), and the number of branch points (**p**) and terminal points (**q**). $n = 30$ neurons per group. **n**, Schematic showing the method for measuring the length of an apical dendrite (dashed line), branch points (Branch Pts, orange) and terminal points (Terminal Pts, green). Scale bars, 100 μm (**b**) and 50 μm (**d, e, j** and **k**). Two-tailed unpaired *t*-test, $***P < 0.001$. Error bars, s.e.m.

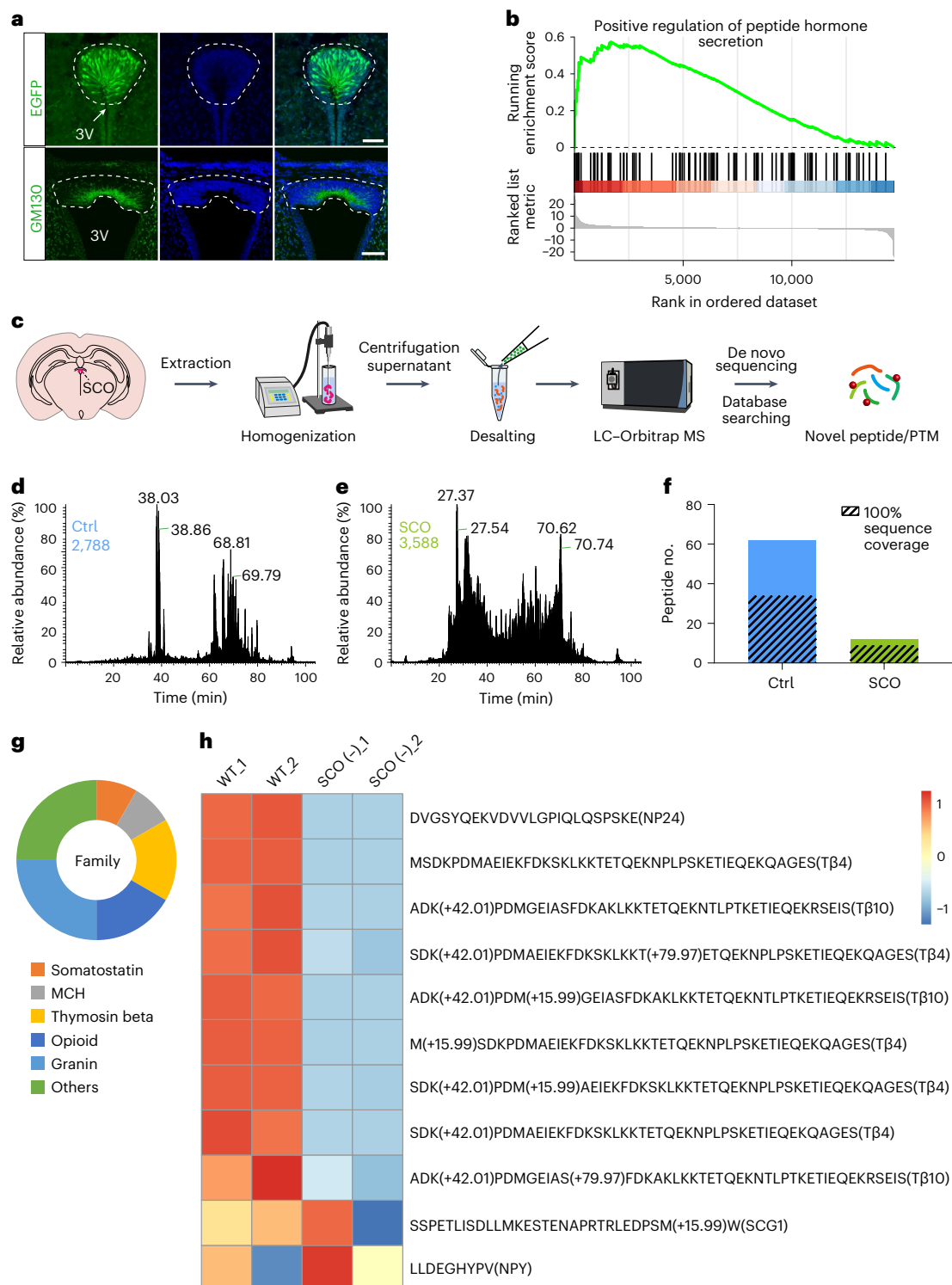


Fig. 6 | Detection of neuropeptides in SCO and their release into CSF. **a**, The morphology of individual SCO cells with polarized long processes extending to the third ventricle (3V, upper row) and gathered Golgi enriched in terminals of polarized processes (GM130, lower row). Dashed lines, SCO margin; green (top row), EGFP fluorescence of SCO cells in *Spso-CreER;Ai47*; green (bottom row), Golgi labeled with anti-GM130; blue, nuclei labeled by Hoechst 33342 (HO). **b**, Gene set enrichment analysis showing that the pathway 'Positive regulation of peptide hormone secretion' was enriched in the SCO. Transcriptomic data were from samples of the SCO and control hippocampus of P0 mice. **c**, The workflow for peptide extraction and peptidomic analysis with LC-MS/MS on an Orbitrap MS platform. PTM, post-translational modification. **d, e**, Peptidomic sequencing results from tandem mass spectra of the control samples (hippocampus, **d**) and

SCO samples (**e**) using a de novo sequencing strategy. Peptide features totaling 2,788 and 3,588 were identified in the SCO and control samples, respectively. **f, g**, The number of peptides identified in the SCO and control samples (**f**, Ctrl, 62 peptides with 34 of them exhibiting 100% sequence coverage; SCO, 12 peptides with 9 of them exhibiting 100% sequence coverage) and peptide family distribution of identified SCO peptides (**g**). MCH, melanin-concentrating hormone. **h**, SCO-secreted T β 4, T β 10 and NP24 in CSF of wild-type (WT) and *Spso-Cre;DTA* mice at E18–P0. WT_1 and WT_2, two samples of mixed CSF of WT mice (~30 pups or embryos per sample); SCO (-)_1 and SCO (-)_2, two samples of mixed CSF of *Spso-Cre;DTA* mice (~30 pups or embryos per sample). Secretogranin-1 (SCG1) and neuropeptide Y (NPY) were detected as internal controls. Scale bars, 50 μm (EGFP, **a**) and 100 μm (GM130, **a**).

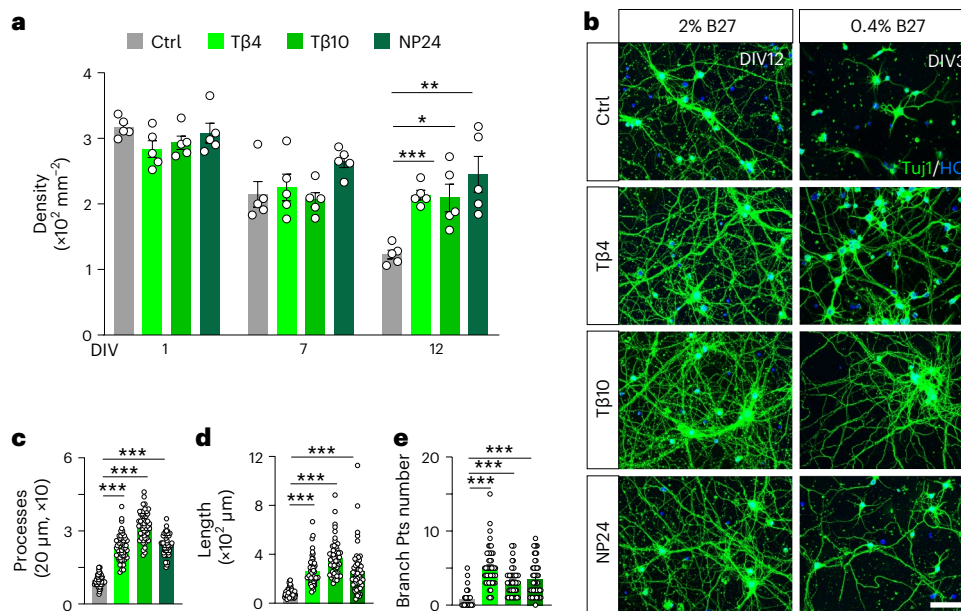


Fig. 7 | SCO-secreted peptides promote neuronal development in vitro. **a**, The density of neurons cultured in the absence (Ctrl) or presence of Tβ4, Tβ10 and NP24 at DIV1, DIV7 and DIV12. $n = 5$ regions per group. **b**, Representative images of neurons in the absence or presence of Tβ4, Tβ10 and NP24 at DIV12 supplied with 2% B27 (left) or at DIV3 supplied with 0.4% B27 (right). Green, neurons labeled with anti-Tuj1; blue, nuclei labeled by Hoechst 33342 (HO). **c**, The number of neurites at 20 μm away from the soma (DIV12) in cultured neurons. Neurons were cultured with 2% B27 in the absence or presence of Tβ4, Tβ10 or NP24. The points

where the neurite intersected a dotted circle were counted. Ctrl, $9.80 \pm 2.45 \mu\text{m}$; Tβ4, $23.26 \pm 5.53 \mu\text{m}$; Tβ10, $32.42 \pm 5.84 \mu\text{m}$; NP24, $24.02 \pm 2.26 \mu\text{m}$ ($n = 50$ neurons per group). **d, e**, Morphological analysis of neurons cultured in the absence or presence of Tβ4, Tβ10 or NP24. Parameters included the length of the apical dendrite (**d**, $n = 50$ neurons per group) and the number of dendritic branch points (**e**, $n = 50$ neurons per group) in neurons cultured with 0.4% B27. Pts, points. Scale bar, 50 μm (**b**). Two-tailed unpaired *t*-test, * $P < 0.05$, ** $P < 0.01$, *** $P < 0.001$. Error bars, s.e.m.

local blood vessels^{2,16}. Ultrastructural analysis has suggested that the SCO is a high-output secretory gland³. A number of proteins, including SCO-spondin, transthyretin and probably fibroblast growth factor, have been reported to be released from SCO cells³. Our proteomic data revealed the presence of SCO-spondin in the CSF of control mice, whereas it was absent from the CSF of SCO-ablated mice. Several oligopeptides derived from the SCO-spondin sequence are bioactive, and their positive roles in neurite growth have been confirmed in vitro^{21,31}. However, it is unknown whether these SCO-spondin oligopeptides are secreted from the SCO under physiological conditions. Although we detected known peptides in CSF, for example, SCG1, NPY and pro-SAAs, we did not detect secretory peptides related to SCO-spondin. Thus, SCO-spondin-derived peptides might be present at low concentrations or may be rapidly degraded by enzymes in CSF after release.

Tβ4, Tβ10 and NP24 are small peptides, and therefore they could potentially reach different cortical layers and act on developing neurons or neuronal progenitors directly through the CSF. We found that all three peptides promoted neuronal development through activation of specific pathways, including neurogenesis and neuronal survival. Some of these functions are similar to those of SCO-spondin, indicating they cooperate to promote growth and development.

The cocktail of peptides that we injected into mice for the rescue experiment included 1 μg of each peptide (that is, 3 μg total). Platelets and leukocytes release Tβ4 into wound fluid with a final concentration of 13 $\mu\text{g ml}^{-1}$ (refs. 32,33). Given that the weight of the developing brain of a mouse pup is 0.2–0.3 g (P2–10), the estimated concentration of Tβ4 that we used in *Sspo-Cre;DTA* mice (1 μg per brain, that is, 3–5 $\mu\text{g ml}^{-1}$) was comparable to the physiological concentration (13 $\mu\text{g ml}^{-1}$). Based on our liquid chromatography (LC)–MS analysis of CSF, we estimated the following concentrations of the peptides: Tβ4, $\sim 5.7 \mu\text{g ml}^{-1}$; Tβ10, $\sim 2.3 \mu\text{g ml}^{-1}$; and NP24, $\sim 0.023 \mu\text{g ml}^{-1}$ (Supplementary Table 3). Considering that enzyme-mediated digestion is always a possibility in CSF and that the amounts of peptides might decrease during collection and

preparation, their concentrations under physiological conditions are probably higher than what we measured.

SCO comprises two cell layers: the ependymal layer, which originates from the epithelium in direct contact with CSF of the third ventricle, and the hypendymal cells situated beneath the ependymal layers of the SCO^{19,34}. We determined that most SCO cells were EGFP⁺ in *Sspo-Cre;Ai47* mice. In addition, the majority of EGFP⁺ cells in SCO were S100β⁺ or Foxj1⁺. The use of *Sspo-CreER;Ai47* mice for sparse labeling of SCO cells revealed individual cell morphologies and confirmed that most EGFP⁺ cells extended processes to the third ventricle, indicating their specialization as ependymal cells in direct contact with CSF.

Emerging evidence has linked abnormal neurodevelopment to hydrocephalus rather than fluid hydrodynamics^{35–38}. Our results indicate that SCO ablation primarily leads to brain malformations during early development, resulting in a thinner cortex and hydrocephalus. The phenotype of our SCO-ablated mice aligns partially with observations in previous congenital or mutant animal models, such as *hyh* mice, *SUMS/np* mice and *H-Tx* rats^{4,8}. The SCO is often dysfunctional or malformed in these models, although they also exhibit dysfunction in non-SCO brain regions, making it uncertain whether the SCO is solely responsible for hydrocephalus. Our observations revealed a thinner cortex in *Sspo-Cre;DTA* mice at E18, before hydrocephalus onset. Our in vitro and in vivo investigations suggest that the SCO plays a vital role in neuronal and cortical development, a finding consistent with prior studies^{20,21}. Nevertheless, some disparities exist between the phenotype observed in our SCO-ablation model and those documented in previous mutant models or animals subjected to SCO immunoblockade³⁹. For instance, *Sspo-Cre;DTA* mice did not develop aqueductal stenosis after specific SCO ablation. Analysis of ependymal cells within the aqueduct revealed no discernible differences between control and *Sspo-Cre;DTA* mice. In homozygous *Sspo-Cre* and *Sspo-CreER* mice, which mimic *Sspo* gene knockout and lack SCO-spondin in their CSF, there was no obvious

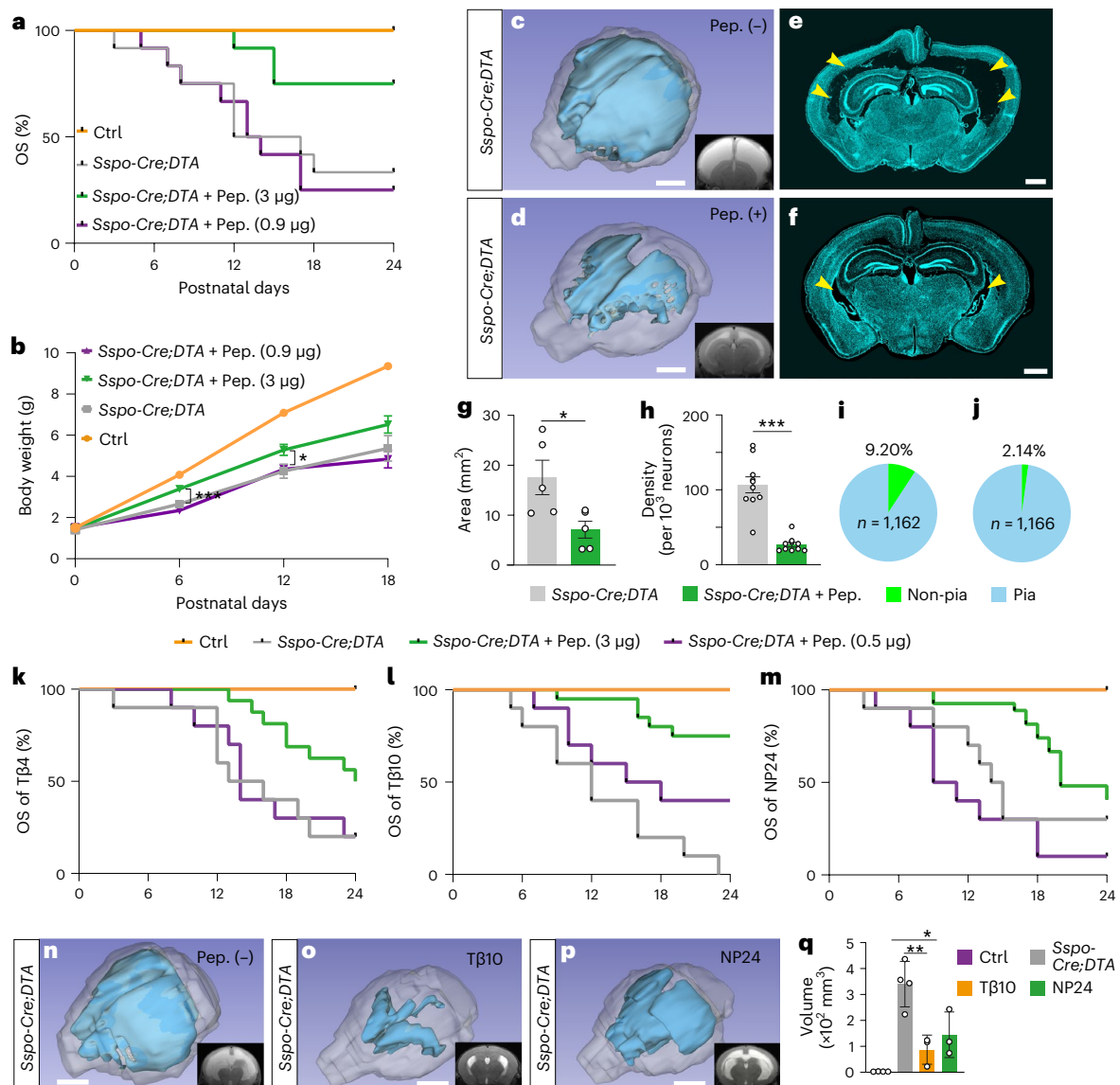


Fig. 8 | SCO-secreted peptides rescue phenotypes in SCO-ablated mice. **a**, The overall survival (OS) of control (orange), *Sspo-Cre;DTA* (gray) and *Sspo-Cre;DTA* mice injected with a cocktail of SCO peptides (Tβ4, Tβ10 and NP24) comprising 0.9 µg (purple) total for all three peptides or 3 µg each time (green); $n = 12$ mice per group. Pep., peptide cocktail. **b**, The body weight of control (orange), *Sspo-Cre;DTA* (gray) and *Sspo-Cre;DTA* mice injected with the SCO peptide cocktail of 0.9 µg (purple) and 3 µg each time (green) at P0, P6, P12 and P18 ($n = 8$ for P0, P6 and P12 mice; $n = 6$ for P18 mice). **c, d**, MRI and 3D reconstruction of the ventricle in *Sspo-Cre;DTA* mice without (c) or with (d, 3 µg) injection of the SCO peptide cocktail at P24. **e–g**, Ventricular area measured from *Sspo-Cre;DTA* mice without (e) or with (f, 3 µg each time) injection of the SCO peptide cocktail at P24. $n = 5$ mice per group (g). Blue, Hoechst 33342 (HO, nuclei); arrowheads, lateral ventricles. **h–j**, The density ($n = 10$ regions per group) and percentage

(i, *Sspo-Cre;DTA* without SCO peptide injection; j, *Sspo-Cre;DTA* mice with cocktail injection, 3 µg each time) of neurons exhibiting non-pia-projected polarization among all labeled neurons. Non-pia, neurons with axons directed toward the corpus callosum; pia, neurons with axons directed toward the pial surface. **k–m**, The overall survival (OS) of control (orange), *Sspo-Cre;DTA* (gray) and *Sspo-Cre;DTA* mice injected with 0.5 µg (purple) or 3 µg (green) of Tβ4 or Tβ10, or NP24 each time. Tβ4, $n = 10, 10, 10$ and 16 mice; Tβ10, $n = 10, 10, 10$ and 20 mice; NP24, $n = 10, 10, 10$ and 27 mice. **n–q**, Three-dimensional reconstruction and quantification of ventricular volume of *Sspo-Cre;DTA* mice after injection of Tβ10 (o, 3 µg each time) or NP24 (p, 3 µg each time) or without injection of SCO peptides (n). In q, $n = 4$ mice for control and *Sspo-Cre;DTA*; $n = 3$ mice for *Sspo-Cre;DTA* + Tβ10 and *Sspo-Cre;DTA* + NP24. Scale bars, 2 cm (c, d and n–p) and 1 mm (e and f). Two-tailed unpaired *t*-test, * $P < 0.05$, ** $P < 0.01$, *** $P < 0.001$. Error bars, s.e.m.

aqueductal stenosis or disruption of ependymal cells or differences in body weight or brain morphology.

The SCO–RF complex is involved in spinal-cord development in zebrafish^{12–14}. Some rodent models, including *hyh* and *H-Tx*, have brain abnormalities including the SCO and RF^{6,11,40,41}. Our results for *Sspo-Cre;DTA* mice revealed apparent abnormalities in the cerebral cortex and lateral ventricles when the SCO was ablated at embryonic stages; however, there was no obvious phenotype in the brain or change in overall survival if the SCO was ablated after P25. These results indicate that the SCO plays a critical role in early brain development, and

its role in adults might differ^{3,9,20}. Previous studies indicated that the monoamine concentration in CSF increases sharply in the absence of RF^{9,42,43}. Further, dysfunction of the adult neurogenic niche also has been proposed and investigated by SCO grafting³. These observations are consistent with our results that the number of SCO cells decreases during embryonic and postnatal development. We cannot exclude the possibility that this decrease is attributable to incomplete experimental ablation of the SCO in adult *Sspo-CreER;DTA* mice.

Although hydrocephalus is commonly attributed to primary defects in CSF homeostasis, emerging evidence suggests

that congenital hydrocephalus may stem not solely from the overproduction of certain factors in CSF but rather from anomalies in neurodevelopment³⁸. In addition, additional evidence has linked abnormal neurodevelopment to hydrocephalus rather than fluid hydrodynamics^{35–38}. Moreover, disruptions in the cerebral cortex or neural stem cells can result in secondary ventricular enlargement without primary defects in CSF circulation^{35,38,44–47}. Abnormal neurogenesis also can arise from defects in the ventricular zone in certain aforementioned animal models of congenital hydrocephalus⁴⁷.

It was recently reported that deletion or mutation of Trim71 in mouse neuroepithelial cells causes prenatal hydrocephalus. Indeed, congenital hydrocephalus mutations can cause abnormalities in neuroepithelial cell differentiation and neurogenesis³⁸. Results from human patients also indicate that genetic disruption of early brain development—rather than impaired CSF circulation—is the primary cause of sporadic congenital hydrocephalus^{35,36}. We observed that E18 *Sspo-Cre;DTA* mice experienced cortex thinning, that is, preceding the onset of hydrocephalus. We posit that a diminution of SCO secretion capacity may lead to abnormalities in neurogenesis, neuronal development and cortex formation that could result in secondary hydrocephalus. Although hydrocephalus in SCO-ablated mice may be linked to SCO–RF defects, concurrent defects in cortical development may contribute to postnatal ventricle expansion.

Online content

Any methods, additional references, Nature Portfolio reporting summaries, source data, extended data, supplementary information, acknowledgements, peer review information; details of author contributions and competing interests; and statements of data and code availability are available at <https://doi.org/10.1038/s41593-024-01639-x>.

References

- Peruzzo, B. et al. Ultrastructural immunocytochemistry and lectin histochemistry of the subcommissural organ in the snake *Natrix maura* with particular emphasis on its vascular and leptomenigeal projections. *Histochemistry* **93**, 269–277 (1990).
- Rodríguez, E. M., Oksche, A. & Montecinos, H. Human subcommissural organ, with particular emphasis on its secretory activity during the fetal life. *Microsc. Res. Tech.* **52**, 573–590 (2001).
- Guerra, M. M. et al. Understanding how the subcommissural organ and other periventricular secretory structures contribute via the cerebrospinal fluid to neurogenesis. *Front. Cell. Neurosci.* **9**, 480 (2015).
- Ortloff, A. R. et al. Role of the subcommissural organ in the pathogenesis of congenital hydrocephalus in the HTx rat. *Cell Tissue Res.* **352**, 707–725 (2013).
- Ortega, E. et al. The value of early and comprehensive diagnoses in a human fetus with hydrocephalus and progressive obliteration of the aqueduct of Sylvius: case report. *BMC Neurol.* **16**, 45 (2016).
- Kohn, D., Chinookoswong, N. & Chou, S. A new model of congenital hydrocephalus in the rat. *Acta Neuropathol.* **54**, 211–218 (1981).
- Somera, K. C. & Jones, H. C. Reduced subcommissural organ glycoprotein immunoreactivity precedes aqueduct closure and ventricular dilatation in H-Tx rat hydrocephalus. *Cell Tissue Res.* **315**, 361–373 (2004).
- Perez-Figares, J. et al. Spontaneous congenital hydrocephalus in the mutant mouse *hyh*. Changes in the ventricular system and the subcommissural organ. *J. Neuropathol. Exp. Neurol.* **57**, 188–202 (1998).
- Caprile, T., Hein, S., Rodríguez, S., Montecinos, H. & Rodríguez, E. Reissner fiber binds and transports away monoamines present in the cerebrospinal fluid. *Mol. Brain. Res.* **110**, 177–192 (2003).
- Muñoz, R. I. et al. The subcommissural organ and the Reissner fiber: old friends revisited. *Cell Tissue Res.* **375**, 507–529 (2019).
- Jiménez, A. et al. A programmed ependymal denudation precedes congenital hydrocephalus in the *hyh* mutant mouse. *J. Neuropathol. Exp. Neurol.* **60**, 1105–1119 (2001).
- Troutwine, B. R. et al. The Reissner fiber is highly dynamic in vivo and controls morphogenesis of the spine. *Curr. Biol.* **30**, 2353–2362 e2353 (2020).
- Rose, C. D. et al. SCO-spondin defects and neuroinflammation are conserved mechanisms driving spinal deformity across genetic models of idiopathic scoliosis. *Curr. Biol.* **30**, 2363–2373 e2366 (2020).
- Orts-Del'Immagine, A. et al. Sensory neurons contacting the cerebrospinal fluid require the Reissner fiber to detect spinal curvature in vivo. *Curr. Biol.* **30**, 827–839 e824 (2020).
- Kousi, M. & Katsanis, N. The genetic basis of hydrocephalus. *Annu. Rev. Neurosci.* **39**, 409–435 (2016).
- Cifuentes, M., Fernández-LLebrez, P., Perez, J., Perez-Figares, J. & Rodríguez, E. Distribution of intraventricularly injected horseradish peroxidase in cerebrospinal fluid compartments of the rat spinal cord. *Cell Tissue Res.* **270**, 485–494 (1992).
- Meinzel, A. et al. The subcommissural organ and Reissner's fiber complex: an enigma in the central nervous system? *Prog. Histochem. Cytochem.* **30**, 1–66 (1996).
- Gobron, S. et al. Subcommissural organ/Reissner's fiber complex: characterization of SCO-spondin, a glycoprotein with potent activity on neurite outgrowth. *Glia* **32**, 177–191 (2000).
- Gobron, S. et al. SCO-spondin: a new member of the thrombospondin family secreted by the subcommissural organ is a candidate in the modulation of neuronal aggregation. *J. Cell Sci.* **109**, 1053–1061 (1996).
- Rodríguez, S. et al. Isograft and xenograft of the subcommissural organ into the lateral ventricle of the rat and the formation of Reissner's fiber. *Cell Tissue Res.* **296**, 457–469 (1999).
- Meinzel, A. SCO-spondin, a glycoprotein of the subcommissural organ/Reissner's fiber complex: evidence of a potent activity on neuronal development in primary cell cultures. *Microsc. Res. Tech.* **52**, 484–495 (2001).
- Brown, D. D. & Afifi, A. K. Histological and ablation studies on the relation of the subcommissural organ and rostral midbrain to sodium and water metabolism. *Anat. Rec.* **153**, 255–263 (1965).
- Voehringer, D., Liang, H.-E. & Locksley, R. M. Homeostasis and effector function of lymphopenia-induced 'memory-like' T cells in constitutively T cell-depleted mice. *J. Immunol.* **180**, 4742–4753 (2008).
- Daigle, T. L. et al. A suite of transgenic driver and reporter mouse lines with enhanced brain-cell-type targeting and functionality. *Cell* **174**, 465–480 e422 (2018).
- Madisen, L. et al. A robust and high-throughput Cre reporting and characterization system for the whole mouse brain. *Nat. Neurosci.* **13**, 133–140 (2010).
- Yulis, C. R. & Muñoz, R. I. Vertebrate floor plate transiently expresses a compound recognized by antisera raised against subcommissural organ secretion. *Microsc. Res. Tech.* **52**, 608–614 (2001).
- Rakic, P. & Sidman, R. L. Subcommissural organ and adjacent ependyma: autoradiographic study of their origin in the mouse brain. *Am. J. Anat.* **122**, 317–335 (1968).
- Hoyo-Becerra, C. et al. The subcommissural organ and the development of the posterior commissure in chick embryos. *Cell Tissue Res.* **339**, 383–395 (2010).
- Roth, L. W., Bormann, P., Bonnet, A. & Reinhard, E. β -Thymosin is required for axonal tract formation in developing zebrafish brain. *Development* **126**, 1365–1374 (1999).

30. Mantri, M. et al. Spatiotemporal single-cell RNA sequencing of developing chicken hearts identifies interplay between cellular differentiation and morphogenesis. *Nat. Commun.* **12**, 1771 (2021).
31. Delétage, N., Le Douce, J., Callizot, N., Godfrin, Y. & Lemarchant, S. SCO-spondin-derived peptide protects neurons from glutamate-induced excitotoxicity. *Neuroscience* **463**, 317–336 (2021).
32. Hannapel, E. & van Kampen, M. Determination of thymosin β 4 in human blood cells and serum. *J. Chromatogr. A* **397**, 279–285 (1987).
33. Frohm, M. et al. Biochemical and antibacterial analysis of human wound and blister fluid. *Eur. J. Biochem.* **237**, 86–92 (1996).
34. Pérez, J. et al. Light-and electron-microscopic immunocytochemical investigation of the subcommissural organ using a set of monoclonal antibodies against the bovine Reissner's fiber. *Histochem. Cell Biol.* **104**, 221–232 (1995).
35. Furey, C. G. et al. De novo mutation in genes regulating neural stem cell fate in human congenital hydrocephalus. *Neuron* **99**, 302–314. e304 (2018).
36. Jin, S. C. et al. Exome sequencing implicates genetic disruption of prenatal neuro-gliogenesis in sporadic congenital hydrocephalus. *Nat. Med.* **26**, 1754–1765 (2020).
37. Hale, A. T. et al. Multi-omic analysis elucidates the genetic basis of hydrocephalus. *Cell Rep.* **35**, 109085 (2021).
38. Duy, P. Q. et al. Impaired neurogenesis alters brain biomechanics in a neuroprogenitor-based genetic subtype of congenital hydrocephalus. *Nat. Neurosci.* **25**, 458–473 (2022).
39. Vio, K. et al. Hydrocephalus induced by immunological blockage of the subcommissural organ-Reissner's fiber (RF) complex by maternal transfer of anti-RF antibodies. *Exp. Brain Res.* **135**, 41–52 (2000).
40. Kiefer, M. et al. The ependyma in chronic hydrocephalus. *Child's Nerv. Syst.* **14**, 263–270 (1998).
41. Wagner, C. et al. Cellular mechanisms involved in the stenosis and obliteration of the cerebral aqueduct of hyh mutant mice developing congenital hydrocephalus. *J. Neuropathol. Exp. Neurol.* **62**, 1019–1040 (2003).
42. Rodríguez, S. et al. Changes in the cerebrospinal-fluid monoamines in rats with an immunoneutralization of the subcommissural organ-Reissner's fiber complex by maternal delivery of antibodies. *Exp. Brain Res.* **128**, 278–290 (1999).
43. Rodríguez, S. & Caprile, T. Functional aspects of the subcommissural organ-Reissner's fiber complex with emphasis in the clearance of brain monoamines. *Microsc. Res. Tech.* **52**, 564–572 (2001).
44. Lehtinen, M. K. & Walsh, C. A. Neurogenesis at the brain-cerebrospinal fluid interface. *Annu. Rev. Cell Dev. Biol.* **27**, 653–679 (2011).
45. Lehtinen, M. K. et al. The cerebrospinal fluid provides a proliferative niche for neural progenitor cells. *Neuron* **69**, 893–905 (2011).
46. Carter, C. S. et al. Abnormal development of NG2⁺ PDGFR- α ⁺ neural progenitor cells leads to neonatal hydrocephalus in a ciliopathy mouse model. *Nat. Med.* **18**, 1797–1804 (2012).
47. Rodríguez, E. M. & Guerra, M. M. Neural stem cells and fetal-onset hydrocephalus. *Pediatr. Neurosurg.* **52**, 446–461 (2017).

Publisher's note Springer Nature remains neutral with regard to jurisdictional claims in published maps and institutional affiliations.

Springer Nature or its licensor (e.g. a society or other partner) holds exclusive rights to this article under a publishing agreement with the author(s) or other rightsholder(s); author self-archiving of the accepted manuscript version of this article is solely governed by the terms of such publishing agreement and applicable law.

© The Author(s), under exclusive licence to Springer Nature America, Inc. 2024

¹Academy for Advanced Interdisciplinary Studies, Peking University, Beijing, China. ²Chinese Institute for Brain Research, Beijing, China. ³Department of Chemistry and School of Pharmacy, University of Wisconsin-Madison, Madison, WI, USA. ⁴School of Basic Medical Sciences, Anhui Medical University, Hefei, China. ⁵State Key Laboratory of Proteomics, National Center for Protein Sciences-Beijing, Beijing Proteome Research Center, Beijing Institute of Lifeomics, Beijing, China. ⁶College of Life Sciences, Nankai University, Tianjin, China. ⁷State Key Laboratory of Cognitive Neuroscience and Learning and IDG/McGovern Institute for Brain Research, Beijing Normal University, Beijing, China. ⁸Department of Laboratory Medicine, Changzheng Hospital, Naval Medical University, Shanghai, China. ⁹Changping Laboratory, Beijing, China. ¹⁰School of Basic Medical Sciences, Capital Medical University, Beijing, China. ¹¹Department of Neurology, First Affiliated Hospital, School of Medicine, Zhejiang University, Zhejiang, China. ¹²National Institute of Biological Sciences, Beijing, China. ¹³Department of Neurosurgery, Xuanwu Hospital, China International Neuroscience Institute, Capital Medical University, Beijing, China. ¹⁴Allen Institute for Brain Science, Seattle, WA, USA. ¹⁵Medical Imaging laboratory of Core Facility Center, Capital Medical University, Beijing, China. ¹⁶Eugene McDermott Center for Human Growth and Development, Department of Bioinformatics, School of Public Health, UT Southwestern Medical Center, Dallas, TX, USA. ✉e-mail: lingjun.li@wisc.edu; sunwenzhi@cibr.ac.cn; woopingge@cibr.ac.cn

Methods

Mice

The use and care of animals followed the guidelines of the Institutional Animal Care and Use Committee at Chinese Institute for Brain Research, Beijing. *DTA* (stock no. 009669) and *Ai14* (stock no. 007914) mice were purchased from the Jackson Laboratory. *Sspo-Cre*, *Sspo-CreER*, *Car3-Cre* and *Spdef-Cre* mouse lines (C57BL/6 background) were developed by our laboratory with the assistance from Biocytogen Pharmaceuticals. The C57BL/6 control mice were purchased from Charles River Laboratory. *Ai47* mice were originally from Dr. Hongkui Zeng's lab at Allen Institute.

Brain excision and preparation of thin sections

Mice (\geq P10) were anesthetized with isoflurane using a vaporizer and were perfused with phosphate-buffered saline (PBS) at room temperature followed by cold 4% paraformaldehyde. Mice younger than P10 were killed by hypothermia (P0–7) before decapitation or were killed by decapitation directly (P0–9). Each brain was excised and postfixed in 4% paraformaldehyde at 4 °C overnight and then dehydrated in 30% sucrose at 4 °C for 2–3 days. After embedding in OCT compound (Tissue-Tek4583, Sakura), each frozen brain was sectioned with a cryostat (Leica, CM3050S) at a thickness of 30 μ m for immunostaining or 15 μ m for RNAscope mFISH.

SCO isolation

Male adult mice (8–10 weeks old) were killed with isoflurane. Each brain was resected and placed in cold PBS (4 °C). Neonatal pups (P0–7) were anesthetized on ice and decapitated for brain dissection. All brains were placed in cold PBS. Hippocampus and SCO were isolated under a stereoscope (Leica M205 FA). All samples for bulk RNA-seq or peptidomic analysis were stored at –80 °C.

Bulk RNA-seq and data analysis

Total RNA was extracted from the SCO and hippocampus or cultured neurons using the RNeasy Micro kit (Qiagen, 74004). The DNA library for sequencing was prepared following the protocol for TruePrep DNA Library Prep kit V2 (SCO and hippocampus) or SMARTer Stranded Total RNA-Seq kit v2 (cultured neurons). RNA-seq raw data were initially filtered with 'FastQC' to obtain clean data after quality control. Clean data were aligned to the reference genome (version GRCm38) downloaded from Gencode by HISAT. Raw counts for each gene were calculated by FeatureCounts. The expression level of detected genes was estimated by DESeq2. A volcano plot was generated by ggplot2 in R, with a cutoff *P* value of <0.01 and absolute value of \log_2 (fold change) of >4 , measured by DESeq2. Gene set enrichment analysis was performed using the ClusterProfiler package in R, with an adjusted *P* value of <0.05 .

RNAscope mFISH

The RNAscope mFISH assay was performed with the RNAscope multiplex fluorescent reagent kit v2 (cat. no. 323100, Advanced Cell Diagnostics) and HybEZ II hybridization system (Advanced Cell Diagnostics). Advanced Cell Diagnostics designed the RNAscope probes for *Car3* (578571-C3, target region: positions 2–1,002 of RNA complementary to the sequence [NM_007606.3](#)), *Spdef* (544421-C2, target region: positions 471–1,400 of RNA complementary to the sequence [NM_013891.4](#)) and *Sspo* (1134541-C1, target region: positions 344–1,232 of RNA complementary to the sequence [NM_173428.4](#)). The positive control (Ms-Ppib, 31391I, Advanced Cell Diagnostics) and negative control (DapB, 310043, Advanced Cell Diagnostics) were applied to evaluate the RNA quality of processed brain sections.

Drug administration

For all CreER mice, tamoxifen (10 mg ml⁻¹, dissolved in a 1:9 mixture of ethanol and sunflower oil) was intraperitoneally injected into mice on or after P5 at 75 μ g g⁻¹ body weight for 5 consecutive days or was injected

intragastrically into neonatal mice (P0–4) at a dosage of 50 μ g (that is, 5 μ l) per mouse daily for 4 consecutive days. For induction of embryonic mice, tamoxifen (100 mg ml⁻¹) was administered to pregnant mice by oral gavage at E10 with a dosage of 5 mg (that is, 50 μ l) once every other day for 4 consecutive days.

EdU staining

To label dividing cells in *Sspo-Cre;DTA* mice at E15, EdU (2 mg ml⁻¹, dissolved in 0.9% saline, Beyotime, ST067) was intraperitoneally injected into their mothers at a dosage of 3 μ l g⁻¹ body weight per mouse. The brain of each *Sspo-Cre;DTA* mouse at E18 was excised and sectioned (30 μ m) after fixation with paraformaldehyde. Brain sections were permeabilized with 0.5% (w/v) Triton X-100 for 30 min and incubated with EdU staining cocktail for 30 min at room temperature (cocktail: Tris-buffered saline (Solarbio, T1080), CuSO₄ (4 mM, Sigma-Aldrich, C8027), sodium ascorbate (20 mg ml⁻¹, Sigma-Aldrich, A7631) and sulfa-cyanine3 azide (3 μ M, Lumiprobe, B1330). Sections were then washed in PBS before being mounted with mounting medium (Electron Microscopy Sciences, 17985).

TUNEL staining

Terminal deoxynucleotidyl transferase dUTP nick end labeling (TUNEL) staining was performed after immunostaining using the One Step TUNEL Apoptosis Assay kit (producing red fluorescence; Beyotime, C1090). Terminal deoxynucleotide transferase (TdT) was diluted with an equal volume of TdT diluent (Beyotime). A TUNEL staining cocktail of diluted TdT (10%) and fluorescent labeling solution (90%) was prepared. Brain sections were incubated with the TUNEL staining cocktail for 1 h at room temperature, washed in PBS and mounted with mounting medium.

Scanning transmission electron microscopy

Mice were perfused with PBS followed by 4% paraformaldehyde. Isolated tissues were post-fixed with 2.5% glutaraldehyde. Tissue blocks containing the aqueduct and spinal central canal were then isolated and post-fixed with 1% osmium tetroxide. The samples were dehydrated through a graded series of ethanol concentrations (50–100%) and infiltrated before embedding in SPI-PON resin (90529-77-4). Araldite resin blocks were sectioned at a thickness of 1.5 μ m and stained with 1% toluidine blue for light microscopy assessment. Ultrathin sections (70 nm) were obtained from selected regions and stained with uranyl acetate and lead citrate. Specimens were imaged with a Hitachi HT7800 transmission electron microscope.

MRI and 3D reconstruction

MRI was performed with a 7.0 T scanner (Pharmascan 70/16, Bruker) equipped with a 23-mm surface coil and a 12-cm-diameter self-shielded gradient system. The user interface consisted of Paravision 5.1 software (Bruker BioSpin) and a Linux PC running Topspin 2.0. Mice were initially anesthetized with 5% isoflurane and 95% O₂ and then maintained with 2% isoflurane and 98% O₂ during imaging. T2-weighted imaging was performed on each brain at different time points with a method of relaxation enhancement using the following parameters: repetition time/echo time 3,500 ms/33 ms, relaxation enhancement factor 4, 21 × 21 mm field of view, 256 × 256 matrix, 20–25 slices and 0.5 mm slice thickness. A 3D slicer software was used for the 3D reconstruction of ventricles and for quantifying ventricle volume.

Virus preparation, purification and infection

To sparsely label neurons in brain, plasmid (*p*)CAG-EGFP was designed to express EGFP under the control of CAG promoter. Each AAV-CAG-EGFP was packaged together with helper plasmids (phelper) and *pRC*. To label cultured neurons, *pFUGWH1-EGFP* was applied, and LV-HI-EGFP was packaged together with *psPAX2* (cat. no. 12260, Addgene) and *pMD2.G* (cat. no. 12259, Addgene). HEK 293T cells were

transfected with the above three-plasmid system for AAVs or LVs using Neofect (TF201201). After purification, the AAVs (10^{12} gc ml⁻¹) and LVs (10^8 – 10^9 TU ml⁻¹) were stored at -80°C for further analysis.

In vivo neuronal labeling and 3D reconstruction

AAV-CAG-EGFP were injected into the lateral ventricle of embryonic mice at a concentration of 10^9 – 10^{10} gc ml⁻¹. Each brain was collected at least 7 days after viral injection. Brain sections with EGFP-expressing neurons were imaged with a VS120 Virtual Slide Microscope (Olympus) and confocal microscope (Leica, SP8). Neuronal morphology was analyzed and reconstructed with Imaris 9.7.1 software (Oxford Instruments). Imaris was used to analyze parameters regarding apical dendrites, including the length of the apical dendrites, the number of dendritic branch points and the number of terminal points.

Morphological analysis of neurons in vitro

Neurons labeled with anti-Tuj1 were imaged by a confocal microscope (Leica, SP8). To quantify neurite density, we first plotted circles along the neuronal soma, 20 μm and 40 μm away from the soma surface, and then counted the number of intersections between neuronal processes and these circles. Finally, the reconstruction of neuronal morphology and the analysis of dendrites were performed as for EGFP-expressing neurons in vivo.

Co-culture of neurons with SCO and in vitro neuron labeling with LVs

Primary cortical neurons, SCO and hippocampus were isolated from *PO-1Sspo-Cre;Ai47* pups. Neurons were cultured on coverslips coated with poly-D-lysine in 24-well plates at a density of 5×10^4 cells per well. The culture medium contained Neurobasal-A (Thermo Fisher, 10888022) supplemented with B27 (2%, Thermo Fisher, 17504044) and GlutaMAX (2 mM, Thermo Fisher, 35050061) with penicillin and streptomycin. Transwells (0.4 μm pore membrane, Corning, 3470) were hung on the top of the coverslip, and an excised SCO from a *Sspo-Cre;Ai47* pup was placed on the pore membrane. Cultured neurons were infected with LVs-H1-EGFP at least 3 days for labeling to assess morphology. For immunostaining, cultured neurons were washed with PBS three times and fixed with 4% paraformaldehyde for 15 min.

Proteomic data analysis

Data-independent acquisition processing was carried out with PEAKS against a refined nonredundant mouse UniProt database with 22,001 entries. Searches utilized a 10-ppm tolerance for peptide masses and 0.02 Da for higher-energy C-trap dissociation (HCD) fragment ion masses. Variable modification included oxidation (methionine), and carbamidomethylation (cysteine) was configured as a fixed modification. The PEAKS quantification module was used to conduct label-free quantitation based on extracted ion chromatograms. Quantitative data were normalized to the summed intensities of all peptide matches.

Digestion of proteins isolated from mouse CSF

CSF samples were diluted with 8 M urea. Each resulting denatured protein sample was chemically reduced with 100 mM dithiothreitol (Roche) at 56°C for 30 min and alkylated using 100 mM iodoacetamide for 1 h. Proteins were digested with trypsin using the filter-aided sample preparation technique⁴⁸. Specifically, 10 μl of each protein mixture was loaded onto a 10 kDa molecular-weight cutoff filter unit that was then centrifuged (14,500g, 15 min). Proteins in the recovered solution were then reduced with dithiothreitol and alkylated with iodoacetamide as noted above. The filter membrane was subsequently washed three times with 50 mM NH_4HCO_3 to eliminate any remaining urea, and proteins were digested with 1 μg trypsin per membrane overnight at 37°C . The resulting tryptic peptides were eluted from the membrane by centrifugation (14,500g, 15 min). An additional 50 μl of 50 mM NH_4HCO_3 was added to the filter membrane, and the membrane

was centrifuged again (14,500g, 15 min). Finally, the two eluates were combined for subsequent analysis.

Proteomics analysis via LC–MS

Samples of tryptic peptides were spiked with the iRT internal standard peptide mix (Biognosys) and analyzed using a nanoLC system (M class, Waters) coupled to an Orbitrap Exploris 480 Mass Spectrometer (Thermo Fisher Scientific). Each sample was loaded onto an Acclaim PepMap trap column (75 $\mu\text{m} \times 2$ cm, 3 μm , C18, 100 \AA , Thermo Scientific) and then separated on a nanoEase BEH C18 column (150 $\mu\text{m} \times 100$ mm, 1.7 μm , C18, 130 \AA , Waters) with solvent A (0.1% formic acid in water) and solvent B (0.1% formic acid in 100% acetonitrile) maintaining a constant flow rate of 600 nl min⁻¹. Peptides were eluted with the following gradient: from 1% to 5% solvent B over 1 min, from 5% to 10% solvent B over 2 min, from 10% to 30% solvent B over 43 min, from 30% to 95% solvent B over 2 min, followed by a 4-min retention at 95% solvent B. This was succeeded by a 1-min transition to 1% solvent B, which was then maintained for 7 min before analysis of the next sample.

The automatic gain control (AGC) target value for the full MS1 scan was set at 300%, with a maximum injection time of 100 ms. For the MS2 scan, the AGC target value was consistently established at 1,000%, paired with a resolution of 30,000 and an injection time of 90 ms. Furthermore, the entire MS scan range was dynamically divided into 60 tandem mass spectrometry (MS/MS) isolation windows, each with a 1-Da overlap, and the collision energy was normalized to 30.

Extraction of endogenous peptides from mouse brain

Individual SCO samples from 120 mice and control hippocampal samples were dissolved in water–methanol–acetic acid (1:90:9, v/v/v) (10 μl per mg tissue). After homogenizing with a Sonic Dismembrator (8 s on, 15 s off, three cycles in total, Fisher Scientific Model FB120), the mixture was centrifuged at 20,000g (20 min, 4°C). The clarified supernatant (200 μl) was aliquoted and loaded onto a 30 kDa molecular-weight cutoff filter (Millipore Amicon Ultra) that had undergone prerinsing as follows: (1) 0.1 M sodium hydroxide, 200 μl ; (2) water/methanol/acetonitrile solution (50:30:20, v/v/v), 200 μl , repeated one time; and (3) water/methanol/acetic acid (1:90:9, v/v/v), 200 μl . For each prerinse, the filter was centrifuged at 15,000g (5 min, 4°C). The supernatant-loaded filters were centrifuged at 15,000g (30 min, 4°C), and the filtrates were collected as the neuropeptide samples (<30 kDa). The flow-through was combined with the previously collected peptide samples (total volume ~600 μl). All samples were then aliquoted and lyophilized. C18 Zip tips (Millipore Sigma) were used for desalting. After lyophilization, the peptide samples were stored at -80°C until LC–MS analysis.

Extraction of peptides from mouse CSF

CSF was collected from 20–30 embryos or neonatal pups of *C57BL6* or *Sspo-Cre;DTA* mice and transferred into two different tubes, with a 55 μl final volume for each sample for subsequent analysis. Each sample was combined with 600 μl water–methanol–acetic acid (1:90:9, v/v/v) and kept on ice for 15 min, then centrifuged at 20,000g for 10 min. Each supernatant was dried in a SpeedVac vacuum concentrator. Each peptide sample was then resuspended in 100 μl water containing 0.1% formic acid, followed by desalting with C18 tips.

LC–Orbitrap MS peptidomics

The peptides extracted from the SCO or control samples were analyzed using a nanoLC system (Dionex UltiMate 3000, Thermo Fisher Scientific) coupled to an Orbitrap Fusion Lumos mass spectrometer (Thermo Fisher Scientific). The samples were reconstituted in a loading solvent of 3% acetonitrile and 0.1% formic acid (v/v). The analytical column was self-made with an integrated emitter tip and dimensions of 75 μm inner diameter \times 17 cm length, 3.0 μm particle size, packed with 1.7 μm , 150 \AA , BEH C18 material (Waters). Solvent A was water containing 0.1%

formic acid, and solvent B was acetonitrile containing 0.1% formic acid. The flow rate was 0.3 $\mu\text{l min}^{-1}$, and the gradient for peptide elution was as follows: 0–16 min, 3% solvent B; 16–20 min, 3–25% B; 20–30 min, 25–45% B; 30–50 min, 45–70% B; 50–56 min, 70–95% B; 56–60 min, 95% B; 60–60.5 min, 95–3% B; 60.5–70 min, 3% B. Data were acquired in top-speed data-dependent mode. Other parameters included: precursor scan AGC, 1×10^6 ; MS/MS scan AGC, 5×10^4 ; isolation window, 1 m/z ; normalized collision energy, 30%; with both HCD and electron-transfer/higher-energy collision dissociation MS/MS analysis.

Peptides extracted from CSF were analyzed with an Orbitrap Q-Exactive HF mass spectrometer (Thermo Scientific) coupled with an online Easy-nLC 1200 nano-HPLC system (Thermo Scientific). Briefly, 5 μl of peptide mixture was loaded on a reversed phase pre-column and then separated on a reversed phase analytical column at a flow rate of 600 nl min^{-1} with a 65-min gradient as reported previously⁴⁹. Peptides were analyzed in data-dependent MS/MS acquisition mode and fragmented by HCD for MS/MS analysis. Detailed parameters for instrument settings can be found in our previous report⁴⁹.

Peptidomic data analysis

Raw data of peptides extracted from the SCO, CSF and corresponding control samples were searched against the mouse neuropeptide database combining NeuroPep and SwePep (337 entries) with PEAKS 8.5 for neuropeptide identification. A mass tolerance of ± 10 ppm was used for precursors; monoisotopic mass tolerance was set to ± 0.02 Da for product ions. HCD fragmentation type and electron-transfer/higher-energy collision dissociation fragmentation were selected individually. An advanced setting that searched against 313 build-in modifications was used for more accurate searching of post-translational modifications. Parameters for confident neuropeptide identification were a score (post-translational modification site confidence) higher than 20, false discovery rate lower than 1% and the presence of at least one unique peptide. Besides the mature neuropeptide database, a custom-built candidate preprohormone database was also used to discover novel neuropeptides, as reported previously⁵⁰.

Raw data for peptides extracted from CSF were processed with PEAKS Studio v8.5 against the neuropeptide database combining Neuropeptides.nl, SwePep, Neuropred.com and Neuropedia.com (487 entries) or UniProt database (downloaded 9 December 2021, encompassing 17,547 entries). Mass tolerance for searches was set to 10 ppm for peptide masses and 0.02 Da for HCD fragment ion masses. Enzyme was set to none. The pyroglutamylation (N-terminal glutamine), oxidation (methionine), amidation (C-terminus), phosphorylation (serine or threonine) and acetylation (lysine) were set as variable modifications. Label-free quantitation based on extracted ion chromatograms was performed using the PEAKS Q module, and quantitative information was exported as .csv files for further bioinformatics processing.

Peptide-based rescue in vitro and in vivo

For the in vitro rescue assay, synthetic T β 4, T β 10 or NP24 (500 $\text{ng } \mu\text{l}^{-1}$, dissolved in 0.9% saline) was mixed with cultured neurons every 3 days from DIV0, and treated neurons were collected between DIV11 and DIV12 for staining. For the in vivo rescue assay, a cocktail containing T β 4, T β 10 and NP24 (1 $\mu\text{g } \mu\text{l}^{-1}$ for each, dissolved in 0.9% saline) or single T β 4, T β 10 or NP24 (0.5 $\mu\text{g } \mu\text{l}^{-1}$ or 3 $\mu\text{g } \mu\text{l}^{-1}$ for each peptide, dissolved in 0.9% saline) was injected into the lateral ventricle of *Sspo-Cre;DTA* mice from P0 for three constitutive days. The control groups included non-injected *Sspo-Cre;DTA* mice and cocktail-injected wild-type mice from the same litter. The body weight and overall survival rate were then calculated. MRI was performed, and each brain was sectioned to measure the volume of lateral ventricles. AAV-CAG-GFP was applied for neuronal labeling for morphological analysis in the brain of *Sspo-Cre;DTA* and control mice treated with SCO peptides.

Statistics and reproducibility

All quantitative data were analyzed using GraphPad Prism (9.0). The two-tailed unpaired Student's *t*-test was used to evaluate the statistical significance of differences between two groups, and the mean \pm s.e.m. is presented with the individual data points shown simultaneously. Statistical significance was analyzed by *P* value: **P* < 0.05, ***P* < 0.01, ****P* < 0.001.

Reporting summary

Further information on research design is available in the Nature Portfolio Reporting Summary linked to this article.

Data availability

All research materials and data are publicly available. New Cre mouse strains are in the process of being donated to the Jackson Laboratory mouse repository for distribution. RNA-seq are publicly available from NCBI GEO (accession numbers GSE214744 and GSE226349) and peptidomic data from IPROX (accession numbers 15E4 and U0Jm). RNA-seq results: these data have been deposited in the publicly available NCBI GEO database and will be released to the public upon publication. The accession information is as follows: SCO bulk RNA-seq (<https://www.ncbi.nlm.nih.gov/geo/query/acc.cgi?acc=GSE214744>), secure token ivatogiazvabpoj; RNA-seq of neurons with peptide incubation (<https://www.ncbi.nlm.nih.gov/geo/query/acc.cgi?acc=GSE226349>), secure token yfkvcygwxbkrvyr; peptidomics data (<https://www.iprox.cn/page/PSV023.html?url=1713509741810ndGU>), accession number 15E4; proteomics data (<https://www.iprox.cn/page/PSV023.html?url=1697721703737jgBn>), accession number U0Jm.

References

- Wisniewski, J. R., Zougman, A., Nagaraj, N. & Mann, M. Universal sample preparation method for proteome analysis. *Nat. Methods* **6**, 359–362 (2009).
- Zhang, P. et al. A dynamic mouse peptidome landscape reveals probiotic modulation of the gut–brain axis. *Sci. Signal.* <https://doi.org/10.1126/scisignal.abb0443> (2020).
- DeLaney, K. & Li, L. Data independent acquisition mass spectrometry method for improved neuropeptidomic coverage in crustacean neural tissue extracts. *Anal. Chem.* **91**, 5150–5158 (2019).

Acknowledgements

We thank lab members in Ge laboratories, B. Samuels and T. Taylor for their feedback and critical reading of the manuscript. We thank Q. Guo, X. Gao and M. Jia in the imaging core of CIBR for assistance with imaging and data analysis. We thank W. Li, S. Huang and R. Shen at the animal core facility for assistance with animal care and purchasing. We thank J. Chen and X. Zhang at the Genomics Center for sequencing and fluorescence-activated cell sorting. We thank the MS facility of the Phoenix Center for use of their instrumentation. We thank F. Huang for suggestions. This work was supported in part by grants from the STI2030-Major Projects (2022ZD0204700), the Natural Science Foundation of China and Beijing Scholars to W.G. (32170964); startup funds from CIBR, the National Key R&D Program of China to C.J. (no. 2021YFA1302601); and a grant from the US National Institutes of Health (NIH, R01DK071801) to L.L. The Orbitrap instruments were purchased through support from an NIH shared instrument grant (NIH-NCRR S1ORRO29531).

Author contributions

W.G. conceived and supervised the project. T.Z., D.A., P.W., L.L., C.J., W.S. and W.G. designed experiments. T.Z. performed most experiments, including mouse genetics, cell ablation, neuronal culture, immunostaining, imaging, RNAscope mFISH, mouse breeding and genotyping, CSF collection and rescue experiments, among others. P.W., Y.X., F.M., Y.Z., T.Z. and C.J. performed peptidomics and proteomics and data analysis. W.G., Z.Z., T.T. and X. Zhang performed SCO bulk

RNA-seq; C.X., D.A. and W.G. analyzed the RNA-seq data. W.G. and T.Z. determined the genes for genetic mouse strains. T.Z. and J.L. assisted in MRI data acquisition and analysis, T.T. assisted in MRI imaging, Z.B. and T.Z. performed AAV viral labeling and peptide injection and assisted in slice imaging. X.-J.C., J.-L.L., J.Y. and L. Zheng assisted in brain slice imaging and electrophysiology. F.L. assisted in neuronal culture. M.Y. assisted in RNA-seq. C.L. assisted in electron microscopy. X. Zou and Z.F. assisted in mouse breeding, genotyping and immunostaining. Z.G. assisted in CSF collection. W.G., W.S., L.L., B.L., C.J., T.H., Z.L., L. Zhang, H. Zhang and H. Zeng provided reagents. T.Z. and W.G. wrote the manuscript. All authors discussed, reviewed and edited the manuscript.

Competing interests

The authors declare no competing interests.

Additional information

Supplementary information The online version contains supplementary material available at <https://doi.org/10.1038/s41593-024-01639-x>.

Correspondence and requests for materials should be addressed to Lingjun Li, Wenzhi Sun or Woo-ping Ge.

Peer review information *Nature Neuroscience* thanks Montserrat Guerra and the other, anonymous, reviewer(s) for their contribution to the peer review of this work.

Reprints and permissions information is available at www.nature.com/reprints.

Reporting Summary

Nature Portfolio wishes to improve the reproducibility of the work that we publish. This form provides structure for consistency and transparency in reporting. For further information on Nature Portfolio policies, see our [Editorial Policies](#) and the [Editorial Policy Checklist](#).

Statistics

For all statistical analyses, confirm that the following items are present in the figure legend, table legend, main text, or Methods section.

- | n/a | Confirmed |
|-------------------------------------|--|
| <input type="checkbox"/> | <input checked="" type="checkbox"/> The exact sample size (n) for each experimental group/condition, given as a discrete number and unit of measurement |
| <input type="checkbox"/> | <input checked="" type="checkbox"/> A statement on whether measurements were taken from distinct samples or whether the same sample was measured repeatedly |
| <input type="checkbox"/> | <input checked="" type="checkbox"/> The statistical test(s) used AND whether they are one- or two-sided
<i>Only common tests should be described solely by name; describe more complex techniques in the Methods section.</i> |
| <input type="checkbox"/> | <input checked="" type="checkbox"/> A description of all covariates tested |
| <input type="checkbox"/> | <input checked="" type="checkbox"/> A description of any assumptions or corrections, such as tests of normality and adjustment for multiple comparisons |
| <input type="checkbox"/> | <input checked="" type="checkbox"/> A full description of the statistical parameters including central tendency (e.g. means) or other basic estimates (e.g. regression coefficient) AND variation (e.g. standard deviation) or associated estimates of uncertainty (e.g. confidence intervals) |
| <input type="checkbox"/> | <input checked="" type="checkbox"/> For null hypothesis testing, the test statistic (e.g. F , t , r) with confidence intervals, effect sizes, degrees of freedom and P value noted
<i>Give P values as exact values whenever suitable.</i> |
| <input checked="" type="checkbox"/> | <input type="checkbox"/> For Bayesian analysis, information on the choice of priors and Markov chain Monte Carlo settings |
| <input checked="" type="checkbox"/> | <input type="checkbox"/> For hierarchical and complex designs, identification of the appropriate level for tests and full reporting of outcomes |
| <input checked="" type="checkbox"/> | <input type="checkbox"/> Estimates of effect sizes (e.g. Cohen's d , Pearson's r), indicating how they were calculated |

Our web collection on [statistics for biologists](#) contains articles on many of the points above.

Software and code

Policy information about [availability of computer code](#)

- | | |
|-----------------|---|
| Data collection | Total RNA was extracted from the SCO and hippocampus or cultured primary neurons using an RNeasy Micro Kit (Qiagen, 74004) following the manufacturer's protocol. The DNA library for sequencing was prepared following the protocol for TruePrep DNA Library Prep Kit V2 (SCO and hippocampus) and SMARTer Stranded Total RNA-Seq Kit v2 (cultured primary neurons). RNA sequencing was performed with an MGI 2000 sequencer under a 100-bp paired-end sequencing strategy. At least 6G of sequencing depth were obtained for each sample. |
| Data analysis | RNA-seq raw data were initially filtered with "FastQC" to obtain clean data after quality control. Clean data were aligned to the reference genome (Version: GRCm38) downloaded from Gencode by HISAT. Raw counts for each gene were calculated by FeatureCounts. The expression level of detected genes was estimated by DESeq2. A volcano plot was generated by ggplot2 in R, with a cutoff of p-value < 0.01 and the absolute value of log ₂ (Foldchange) > 4, measured by DESeq2. The heat map was generated by the heatmap function with the z-score of each gene. Gene Set Enrichment Analysis (GSEA) was performed using the ClusterProfiler package in R, with an adjusted p-value < 0.05. |

For manuscripts utilizing custom algorithms or software that are central to the research but not yet described in published literature, software must be made available to editors and reviewers. We strongly encourage code deposition in a community repository (e.g. GitHub). See the Nature Portfolio [guidelines for submitting code & software](#) for further information.

Data

Policy information about [availability of data](#)

All manuscripts must include a [data availability statement](#). This statement should provide the following information, where applicable:

- Accession codes, unique identifiers, or web links for publicly available datasets
- A description of any restrictions on data availability
- For clinical datasets or third party data, please ensure that the statement adheres to our [policy](#)

All research materials and data are publicly available.

Human research participants

Policy information about [studies involving human research participants and Sex and Gender in Research](#).

Reporting on sex and gender

N.A.

Population characteristics

N.A.

Recruitment

N.A.

Ethics oversight

N.A.

Note that full information on the approval of the study protocol must also be provided in the manuscript.

Field-specific reporting

Please select the one below that is the best fit for your research. If you are not sure, read the appropriate sections before making your selection.

Life sciences Behavioural & social sciences Ecological, evolutionary & environmental sciences

For a reference copy of the document with all sections, see [nature.com/documents/nr-reporting-summary-flat.pdf](https://www.nature.com/documents/nr-reporting-summary-flat.pdf)

Life sciences study design

All studies must disclose on these points even when the disclosure is negative.

Sample size

We usually used over 5 animals/samples for our experiments if no statistical methods were used (see our statement).

Data exclusions

We don't exclude our experimental animals if there is not particular reason, e.g., mice died during experiments.

Replication

All the experiments were replicated at least twice.

Randomization

We randomly chose the animals for our experiments if they were at right ages and healthy.

Blinding

Blinding test was not feasible in this study.

Reporting for specific materials, systems and methods

We require information from authors about some types of materials, experimental systems and methods used in many studies. Here, indicate whether each material, system or method listed is relevant to your study. If you are not sure if a list item applies to your research, read the appropriate section before selecting a response.

Materials & experimental systems

n/a	Involvement
<input type="checkbox"/>	<input checked="" type="checkbox"/> Antibodies
<input checked="" type="checkbox"/>	<input type="checkbox"/> Eukaryotic cell lines
<input checked="" type="checkbox"/>	<input type="checkbox"/> Palaeontology and archaeology
<input type="checkbox"/>	<input checked="" type="checkbox"/> Animals and other organisms
<input checked="" type="checkbox"/>	<input type="checkbox"/> Clinical data
<input checked="" type="checkbox"/>	<input type="checkbox"/> Dual use research of concern

Methods

n/a	Involvement
<input checked="" type="checkbox"/>	<input type="checkbox"/> ChIP-seq
<input checked="" type="checkbox"/>	<input type="checkbox"/> Flow cytometry
<input type="checkbox"/>	<input checked="" type="checkbox"/> MRI-based neuroimaging

Antibodies

Antibodies used	The primary antibodies used in this study included mouse anti-NeuN (1:1,000, Millipore, MAB377, clone A60), rabbit anti-TBR1 (1:150, Abcam, ab31940), mouse anti-Tuj1 (1:1,000, R&D, MAB1195), mouse anti-SATB2 (1:200, Abcam, ab51502), mouse anti-MAP2 (1:500, EMD Millipore, MAB3418), rat anti-CTIP2 (1:200, Abcam, ab18465), mouse anti-GFP (1:500, Abcam, ab13970), rabbit anti-S100 β (1:200, Abcam, ab52642), mouse anti-Foxj1 (1:50, Thermo Fisher, 14996582), mouse anti- β -Catenin (1:50, Santa Cruz Biotech, sc7963), and rabbit anti-GM130 (1:200, Abcam, ab52649). Alexa Fluor-conjugated secondary antibodies included AF488 goat anti-mouse IgG (1:500, Thermo Fisher, A11001), AF546 goat anti-mouse IgG (1:500, Thermo Fisher, A11003), AF488 goat anti-rabbit IgG (1:500, Thermo Fisher, A11008), AF546 goat anti-rabbit IgG (1:500, Thermo Fisher, A11010) and F488 donkey anti-rat IgG (1:500, Thermo Fisher, A21208).
Validation	All the primary antibodies were valid for the indicated species and applications based on the statement of manuscript's website or relevant citation.

Animals and other research organisms

Policy information about [studies involving animals](#); [ARRIVE guidelines](#) recommended for reporting animal research, and [Sex and Gender in Research](#)

Laboratory animals	Mice (C57BL/6, Sspo-Cre, Sspo-CreER, Spdef-Cre, Car3-Cre, Ai47, Ai14, DTA), male and female, P0-P365.
Wild animals	N.A.
Reporting on sex	Sex was not considered in this study.
Field-collected samples	N.A.
Ethics oversight	All animal experiments were in accordance with protocols approved by the Institutional Animal Care and Use Committee at Chinese Institution for Brain Research, Beijing. Our animal protocols are LARC-T025 and 2021-003.

Note that full information on the approval of the study protocol must also be provided in the manuscript.

Magnetic resonance imaging

Experimental design

Design type	To scan whole brain structure of mice
Design specifications	The whole brain of Sspo-Cre;DTA and control mice were performed T2-weighted scanning at ages of P3, P9 and P24
Behavioral performance measures	N.A.

Acquisition

Imaging type(s)	Structural
Field strength	7.0
Sequence & imaging parameters	Pulse sequence type in this study was spin echo and image type was T2-weighted (T2W) with a method of relaxation enhancement (RARE), using the following parameters:repetition time (TR)/echo time (TE) 3500ms/33ms, 4 RARE factor, 21 \times 21mm field of view (FOV), 256 \times 256 matrix, 20–25 slices, and 0.5-mm slice thickness.
Area of acquisition	A whole brain scan was used in this study.
Diffusion MRI	<input type="checkbox"/> Used <input checked="" type="checkbox"/> Not used

Preprocessing

Preprocessing software	Paravision 5.1 software (Bruker BioSpin) and a Linux PC running Topspin 2.0 provided the user interface.
Normalization	N.A.
Normalization template	N.A.
Noise and artifact removal	N.A.
Volume censoring	N.A.

Statistical modeling & inference

Model type and settings	We evaluated the brain malformation and hydrocephalus of mice brains from T2-weighted images.
Effect(s) tested	N.A.
Specify type of analysis:	<input checked="" type="checkbox"/> Whole brain <input type="checkbox"/> ROI-based <input type="checkbox"/> Both
Statistic type for inference (See Eklund et al. 2016)	N.A.
Correction	N.A.

Models & analysis

n/a	Involvement in the study
<input checked="" type="checkbox"/>	<input type="checkbox"/> Functional and/or effective connectivity
<input checked="" type="checkbox"/>	<input type="checkbox"/> Graph analysis
<input checked="" type="checkbox"/>	<input type="checkbox"/> Multivariate modeling or predictive analysis